Waring MJ, Chen H, Rabow AA, Walker G, Bobby R, Boiko S, Bradbury RH, Callis R, Clark E, Dale E, Daniels DL, Dulak A, Flavell L, Holdgate G, Jowitt TA, Kikhney A, McAlister M, Mendez J, Ogg D, Patel J, Petteruti P, Robb GR, Robers MB, Saif S, Stratton N, Svergun DI, Wang W, Whittaker D, Wilson DM, Yao Y. Potent and selective bivalent inhibitors of BET bromodomains. *Nature Chemical Biology* 2016

Potent and selective bivalent inhibitors of BET bromodomains

Authors

Michael J. Waring,[1,2*†] Huawei Chen,[3†] Alfred A. Rabow,[1†] Graeme Walker,[1†] Romel Bobby,[1] Scott Boiko,[3] Rob H. Bradbury,[1] Rowena Callis,[1] Edwin Clark,[3*] Ian Dale,[1] Danette L. Daniels,[4] Austin Dulak,[3] Liz Flavell, [1] Geoff Holdgate,[1] Thomas A. Jowitt,[5] Alexey Kikhney,[6] Mark McAlister,[1] Jacqui Méndez,[4] Derek Ogg,[1] Joe Patel,[3] Philip Petteruti,[3] Graeme R. Robb,[1] Matthew B. Robers,[4] Sakina Saif,[3] Natalie Stratton,[1] Dmitri I. Svergun,[6] Wenxian Wang,[3] David Whittaker,[1] David M. Wilson,[1] Yi Yao.[3]

[1] AstraZeneca, Mereside, Alderley Park, Macclesfield, Cheshire, SK10 4TG, U.K.
[2] Northern Institute for Cancer Research, School of Chemistry, Newcastle University, Bedson Building, Newcastle upon Tyne, NE1 7RU, United Kingdom
[3] AstraZeneca, Gatehouse Park, Waltham, MA 02451, U.S.A.
[4] Promega Corp., 2800 Woods Hollow Road, Madison, WI 53711, U.S.A.
[5] Wellcome Trust Centre for Cell-Matrix Research, University of Manchester, Manchester, M13 9PT, U.K.
[6] European Molecular Biology Laboratory, Hamburg Outstation, c/o DESY, Notkestrasse 85, Hamburg, 22603, Germany.
*Correspondence related to the manuscript to: Prof. Michael J. Waring: Tel. +44 (0)191 208 8591; Email: mike.waring@newcastle.ac.uk; correspondence relating to the AstraZeneca programme to Edwin Clark: Tel +1 781 839 4983; Email: edwin.clark@astrazeneca.com
†These authors contributed equally to this work.

Abstract

Proteins of the bromodomain and extraterminal (BET) family, in particular bromodomain containing protein 4 (BRD4), are of significant interest as biological targets. BET proteins contain two separate bromodomains and existing inhibitors bind monovalently. Here we describe the discovery and characterisation of probe compound, biBET-6, capable of engaging both bromodomains simultaneously in a bivalent, *in cis* binding mode. We provide evidence for this using a variety of biophysical and cellular experiments. The bivalent binding results in very high cellular potency for BRD4 binding and pharmacological responses, for example, disruption of BRD4 / mediator complex subunit 1 foci with an EC_{50} of 100 pM. These compounds will be of significant utility as BET / BRD4 chemical probes. This work illustrates a novel concept in ligand design, simultaneous targeting of two separate domains with a drug-like small molecule, providing precedent for a potentially more effective paradigm for developing ligands for other multi-domain proteins.

Introduction

The bromodomain (BRD) containing proteins are a family of proteins responsible for reading epigenetic acetylated lysine marks on histones and are rapidly emerging as a target class amenable to inhibition with small molecules[1]. The bromodomain and extraterminal (BET) sub-family are perhaps the most widely explored of the class[2]. Initially identified as a result of phenotypic screening for modulation of Apolipoprotein A1, subsequent target identification and compound optimisation has revealed multiple small molecule inhibitors of BET BRDs, which have progressed to preclinical and clinical evaluation[3,4,5].

The BET family consists of four proteins, termed BRD2, BRD3, BRD4 and BRDT[6]. Each of these proteins contain two separate BRDs[7]. Existing chemical probes, such as i-BET762 (**1**) (**Fig. 1a**), do not show selectivity for individual family members and are monovalent ligands, which bind monovalently to both BRDs within each protein with a 2:1 stoichiometry. These chemical probes have been critical to elucidating underlying BET biology. In the oncology field, the existence of tumour types driven by BRD4 fusion mutations[5] and those in which critical oncogenes such as *c-Myc* are regulated by BRD4[8,9] has led to great interest in BRD4 / BET inhibitors and a number are currently progressing in early clinical trials[10].

Here we describe our discovery of a new class of bivalent BET inhibitors, culminating in the chemical probe biBET-6. We have shown, with a combination of techniques, that they act *via* an *in cis* binding mode, simultaneously engaging both BRDs in a single protein. This binding mode results in significantly enhanced cellular potency and slow dissociation kinetics resulting in the most potent cellular probe for BET proteins described to date.

Results

Discovery of bivalent BET inhibitors

As part of a programme to identify down regulators of the androgen receptor (AR), the development candidate AZD3514 was recently reported[11,12]. AZD3514 displayed binding to the AR and cellular AR down regulation (DR) at similar and reasonably high concentrations. We therefore embarked on a chemistry campaign focused on increasing potency, leading to the discovery of compounds such as **2**, which possessed increased AR DR potency but showed a disconnect between binding and cellular potency values (**Fig. 1a**). Moreover, it was revealed that these compounds also effected DR of the estrogen receptor-α (ER) at concentrations comparable to those seen for the AR, suggesting that there was indirect and unknown pharmacology driving both of these phenotypes.

These findings led us to consider what the direct target of the compounds might be. Comparison of these structures with known BET inhibitors led us to speculate that elements of our compounds might be capable of BRD binding and this might have been the cause of the observed pharmacology. For instance, the chlorotriazole motif contained within the triazolopyridazine (TPDZ) of **2** could be overlayed with the methyltriazole of **1**. Alternatively, the piperazinone N-methyl and carbonyl groups could be overlayed with those of acetyl lysine. Compound **2** was subsequently tested in a panel of BRD assays[13], revealing activity against the BET family {pK_d values of 7.2 against BRD4 isolated bromodomain 1 [BRD4(1)], 6.1 against bromodomain 2 [BRD4(2)], **Fig. 1b**}. Further profiling in cells showed that **2** caused DR of c-Myc (**Fig. 1c**) and inhibition of tumour cell growth in a manner consistent with sensitivity to BRD4 inhibition, i.e. complete cell growth inhibition and a strong induction of apoptosis in BRD4 sensitive MM.1S, MOLP-8, MV-4-11, and RS4;11 cells (pGI_{50} 7.3, 7.2, 7.4 and 6.8 respectively); partial growth inhibition without discernible apoptosis induction in less sensitive K-562 (pGI_{50} 6.0).

We found that **2** also has weak activity for BRD4(1) and BRD4(2), but with values comparable to its AR binding and DR potencies. It is interesting to note that an independent analysis has subsequently revealed that **2** has a similar pharmacological profile to BET inhibitors in cancer cell panels[14,15]. The

ability of BET inhibitors to effect inhibition of AR mediated signalling[16] and ER DR[17] has subsequently been reported.

Induced dimerisation of BRD4(1) by X-ray crystallography

Our structural hypotheses implied that either the TPDZ or the piperazinone group could engage the BET acetyl lysine pocket. Solving the co-crystal structure of **2** in the presence of BRD4(1) (pdb code 5AD2, **Supplementary Table 1** and **Supplementary Fig. 1**) revealed a remarkable, compound-induced dimerisation of two BRD4(1) molecules within the crystal lattice, with **2** spanning both acetyl lysine binding sites (**Fig. 2a**). The TPDZ group was observed to make hydrogen bonds with the side chain of Asn140 and a structural water molecule at the base of the pocket (**Fig. 2b**). The piperidine ring projected over the WPF shelf (W81, P82, F83)[3] and the aryl ring contacted the WPF shelf of the second bromodomain with the pendant piperazinone engaging the second binding site. The piperazinone formed a strong H-bond with a structural water molecule and a weaker polar contact with the side chain of Asn140 (**Fig. 2c**).

Optimisation of bivalent binding

The dimeric X-ray structure was consistent with the structure activity relationships (SAR) we had observed in cellular assays with changes to both ends of the molecule that removed the observed interactions with the acetyl lysine pocket resulting in a loss of potency. For example, replacement of the TPDZ chloro substituent (postulated to mimic the methyl of acetyl lysine) with an alternative methyl mimic, such as a trifluoromethyl group (**3**) retained activity; whereas deletion of the substituent (**4**) led to a loss of BRD4 affinity and cellular potency (**Fig. 3a**). Moving the carbonyl substituent of the piperazinone to the 3-position (**5**), thereby disrupting the interaction with the critical Asn residue, led to loss of cellular potency but with retained BRD4(1) binding affinity.

We reasoned that, in a bivalent complex, one of the BRD binding motifs may possess higher affinity than the other and pseudo-symmetrical compounds may have further increased potency. The data for binding to BRD4(1) for **4** and **5** suggested that the TPDZ was the more potent warhead, given the greater loss of potency for **4** compared to **5**. Accordingly, we designed and synthesised compounds with a second TPDZ motif replacing the piperazinone of **3**, resulting in pseudo-symmetrical compounds **6** and **7** (**Fig. 3b**). In this case, a methoxy substituted TPDZ was used as it was found that this substituent led to improved physical properties without a detriment to potency. These compounds showed increased potency against BRD4(1), along with further increased potency against the tandem domain construct (pK_d 11, **Fig. 3c**) and in cells (e.g. pEC_{50} 9.2 and >9.3 for c-Myc DR for **6**). The compounds also retained a similar BRD selectivity profile to **3** (**Supplementary Fig. 2**). These cellular potencies are, to the best of our knowledge, the highest reported to date for BRD4 inhibitors, being more than two orders of magnitude more potent than **1**. Rearrangement of the acetyl lysine mimic of the triazolopyridazine coupled with inversion of the stereocentre (**8**) led to significantly reduced BRD4 activity and no detectable ER downregulation, providing an inactive control and further evidence that the observed pharmacology was BRD4 driven. Compound **7** proved too insoluble (<1 μM) for further biophysical characterisation and so further studies focused on **6**, which showed good in vitro ADME properties (**Supplementary Table 2**).

In selectivity panels of 32 bromodomains[13], 123 kinases and 147 secondary pharmacology assays, **6** showed selectivity for the BET family compared with other BRDs (**Supplementary Fig. 2**), no detectable kinase activity at 1 μM (**Supplementary Table 3**) and only 10 of the other secondary pharmacology assays registered potencies below 10 μM (**Supplementary Table 4**) with the most potent being 5HT1B receptor (agonist EC_{50} 0.93 μM, selectivity ratio of 1400 fold to BRD4 potency).

The X-ray structure of **6** with BRD4(1) revealed a similar dimeric structure to that observed with **2** (**Fig. 3d**, pdb code 5AD3, **Supplementary Table 5**, **Supplementary Fig. 3**). The triazolopyridazine groups were seen to make differential interactions in the two bromodomains. One group made similar contacts with Asn140 and the structural waters as observed with **2**, while in the other binding site, the hydrogen bonds to the waters were observed but that to Asn140 was not (**Supplementary Fig. 4**). The latter is not as typically seen with triazolopyridazine structures and may not represent the mode of engagement

that occurs in solution. Indeed, a close analogue of **6** was observed to engage with Asn140 and the key structural water with both TPDZs under the same conditions (**Supplementary Fig. 5**).

Determination of compound binding mode

The enhanced potency of **6** and **7** against the tandem domain constructs and in cellular assays, led us to believe that the bivalent binding observed in the X-ray structure was relevant to their cellular mechanism of action. Given the presence of two bromodomains in full-length BRD4, there are several possible binding modes for such bivalent compounds. In one mode, the compounds may bind with 2:1 stoichiometry with one compound occupying each BRD in the same way as observed for monovalent compounds such as **1** (**Supplementary Fig. 6a**). This was considered unlikely to be the sole binding mode as it would not explain observed SAR or the difference in behavior relative to monovalent ligands such as **1**. Alternatively, the two warheads of a single molecule may bind to a bromodomain inducing an *in cis* complex (**Supplementary Fig. 6b**) or an *in trans* dimer (**Supplementary Fig. 6c**). In the case of *in trans* binding, multiple possibilities exist with different combinations of each warhead binding to BD1 and BD2. In addition, higher order multimeric species may form.
A computational model of the full-length protein based on the structure of **2** using a homology model of BD2 and a simulated interdomain region showed that formation of an *in cis* complex was possible (**Supplementary Fig. 6d**) as well as an *in trans* dimer (**Supplementary Fig. 6e**) (see Online Methods section). Under physiological conditions any one or more of these states may exist and the relative populations of each are likely to vary with both protein and compound concentration. In particular, the 2:1 complex is likely to dominate at very high concentrations as the protein becomes saturated with ligand.

Binding of 1 and 6 to BRD4(1,2) tandem domain by NMR

The first step in elucidating the binding mode of the compounds was to establish whether both bromodomains were engaged by the ligands in solution. We recorded a series of two-dimensional transverse relaxation optimised ^{1}H-^{15}N heteronuclear single quantum coherence (TROSY HSQC) NMR spectra on tandem domain BRD4(1,2) (residues 44-460) in complex with monovalent **1** and bivalent **6** at ligand to protein ratios of 1:1 and 2:1 (**Fig. 4a**). BRD4(1,2) showed a chemical shift dispersion characteristic of a structured protein with an unstructured region (**Supplementary Fig. 7a**). Tryptophan resonnances could be assigned by comaprison of the individual spectra for the isolated first (BD1) and second (BD2) bromodomains with that of the tandem domain (**Supplementary Fig. 7b**) allowing the W374 resonance in BD2 to be assigned and the remaining three tryptophan resonnances to be ascribed to BD1 (see Online Methods section). Independent confirmation of resonances from BRD4(2) was obtained employing segmental isotope labelling of the C-terminal bromodomain of BRD4(1,2)[18].
Shifts in the signals for both domains were seen clearly in the presence of **1** in the slow-exchange regime typical for tight binding (**Fig. 4a**, **Supplementary Fig. 7c**). Similarly, upon titration of **6**, engagement of both domains simultaneously was observed. Given the difference between the affinities of **6** measured for BRD4(1) and BRD4(2), this observation is inconsistent with monovalent binding, where a greater proportion of engagement with BD1 would be expected. In addition, binding of **6** significantly changed a number of other peaks in the spectrum, which were very different to those observed for **1**. Together, these observations show that **6** binds to both BD1 and BD2 acetyl lysine pockets and suggest that its binding mode is different to that of **1** (for further discussion, see Supplementary Note 1).

Characterisation of complexes of 1 and 6 by AUC and SAXS

Analytical ultracentrifugation (AUC)[19] for apo BRD4(1,2) showed a sedimentation coefficient ($s_{20,W}$) of 2.46±0.05 S and an f/f_0 ratio of 2.2, consistent with a dispersed monomer of highly extended conformation. In the presence of **1**, the sedimentation coefficient was very similar to that of apo BRD4(1,2) indicating no change in oligomeric state or gross conformation (**Fig. 4b**). In the presence of **6**, however, dramatic effects on the peak profiles and sedimentation coefficients were observed. At 1:1, two peaks were observed; one with a similar sedimentation coefficient to apo BRD4(1,2) and a faster sedimenting species (coefficient 2.8 S). To test whether these changes were due to conformational changes in the molecule, the data were analysed using a c(s,f/f_0) model[20]. The contour plot of the distribution of frictional ratios across the peaks of the 1:1 complex with **6** (**Fig. 4c**) showed

that the frictional ratio of the species within the two peaks varied from ~2.2 for the first peak to ~1.4 for the second, indicative of a conformational tightening of the molecule. At 2:1 ligand:protein ratio, the same analysis revealed the formation of smaller populations of dimeric species (**Supplementary Fig. 8**). These sedimentation analyses indicated that binding of **6** elicits a large conformational change in BRD4 resulting in a more compact shape and also suggested formation of a small proportion of dimeric species at higher ligand concentrations. These species likely represent *in cis* and *in trans* interactions between the BRDs induced directly by **6**.

Small angle X-ray scattering (SAXS)[21] studies on apo BRD4(1,2) showed it to be largely monomeric at concentrations below 1 mg mL^{-1} (at increasing concentrations, the protein tended to aggregate in both presence and absence of compound and so the data were extrapolated to zero concentration for analysis) and was flexible in solution. *Ab initio* and ensemble optimisation method (EOM) analysis[22], suggested it was extended (**Fig. 4d**). This changed very little upon addition of **1**. In the presence of **6**, the protein became progressively and significantly more compact. The most compact complex was obtained at 2:1 ligand:protein ratio, indicating the greatest population of *in cis* complex at this stoichiometry.

We calculated distributions of interdomain distances (between Ile 110 in BD1 and Met 425 in BD2) from the 100 out of 10,000 theoretical models best fitting the experimental data (see Online Methods section). In the apo protein, an average interdomain distance of 140±12 Å was observed (**Fig. 4d**) representing an absence of contacts between the two domains and the complex with **1** showed only slightly smaller distances. In contrast, the complex with **6** had significantly shorter interdomain separations (average of 84±18 Å and 63±18 Å for the 1:1 and 2:1 complexes respectively). The radii of gyration (R_g) showed a similar picture (**Supplementary Table 6**). These data are strongly suggestive of a different binding mode of **6** compared to **1** and one in which a significant change in protein conformation is induced.

The comparable interdomain distance in the BD1 dimeric crystal structure of **6** was 38 Å. Hence, this is consistent with the formation of a complex with BD1 and BD2 in similar proximity in the SAXS experiment. Since the R_g values for **6** are significantly lower than those for the apo protein and complexes with **1**, it is reasonable to assume that the complex with **6** is mostly monomeric. Taken together, this is highly suggestive of the formation of a significant population of an *in cis* complex. However, it must be noted that these data are extrapolated to infinite dilution and therefore may not be reflective of the binding mode under cellular conditions, under which higher order multimers may form.

Cellular mode of action and pharmacology

We developed bioluminescence resonance energy transfer (BRET) systems[23] in HCT116 and HEK293 cells to monitor interaction with chromatin using Halo-tagged histone H3 and a Nanoluciferase fusion protein with either BRD4(1) or full-length BRD4. Compound **1** displaced both isolated BRD4(1) and full-length protein with the similar potency (**Fig. 5a**). In contrast, **6** showed a remarkable (4 orders of magnitude) enhancement in potency for displacement of full-length BRD4 relative to BRD4(1) (pIC_{50} 9.6 and 5.6 respectively). This potency increase provides evidence that the bivalent mechanism also operates in cells and is responsible for the cellular potency of **6**. Analogous experiments comparing full length wild-type BRD4 to the N433F point-mutant provided compelling evidence of the need to engage BD2 specifically to exert this effect (**Fig. 5a**). The mutant showed a similar chromatin displacement response to isolated BRD4(1) in these experiments and **6** had a comparable potency to **1** (pIC_{50} 6.6 and 6.8 respectively). The binding of BRD4 to acetylated chromatin is believed to be dominated by BD1 interactions[24] and the N433F mutation is known to provide a steric barrier to engagement of the BRD4(2) acetyl lysine pocket[25] and so bivalent engagement of both acetyl lysine pockets by **6** is required to exert the increased potency.

To detect if binding of **6** produced a conformational change within BRD4, a NanoBRET BRD4 biosensor, was constructed consisting of the two tandem bromodomains, BD1 and BD2, expressed between HaloTag and NanoLuc fusions (**Fig. 5b**). The signal in this conformational biosensor showed no change after treatment of **1** compared to basal levels. Treatment with **6**, however, showed a significant increase in signal at the concentration causing chromatin displacement. The plateau of signal observed with **6** was highly suggestive of an *in cis* binding mechanism. To study this further, a point mutant within BD1, N140F, was made within the biosensor. This mutant biosensor demonstrated a similar basal level signal to the wild-type, no change in signal after treatment with **1** (**Fig. 5b**) and,

strikingly, no response to **6**. Together these data support an *in cis* binding mechanism of **6** to both bromodomains within a single BRD4 protein.

To analyze intracellular target engagement of the compound with BRD4, BRET was then monitored utilising a fluorescently labeled version of **1** in conjunction with Nanoluciferase fusion constructs of BRD4(1), full-length BRD4 and BRD4(N433F) competitively displaced with varying concentrations of test compound (**Fig. 5c**)[26]. Again, **6** showed a remarkable difference in potency for displacement of tracer from full-length BRD4 relative to BRD4(1) and BRD4(N433F) (pIC_{50} 9.0, 5.8 and 6.3 respectively). The same was not observed for **1**. As anticipated, comparative experiments assessing intracellular target engagement (**Supplementary Fig. 9**) and acetylated histone displacement (**Supplementary Fig. 10**) for the other BET family members showed similar effects.

Intracellular residence times of **1** and **6** were then determined, in which cells expressing Nanoluciferase fusions of BRD4 were incubated with the indicated single concentration, equivalent to the corresponding IC_{50} value, of compound for 3 hours [1 nM **6** used for full length BRD4 and 1 μM **6** used for BRD4(N433F) and BRD4(1)]. Following compound equilibration and multiple wash steps, 1 μM tracer was added to intact cells and the dissociation of **1** and **6** were measured[26]. Compounds **1** and **6** showed rapid dissociation from BRD4(1) and BRD4(N433F), whereas **6** showed slower displacement from full-length BRD4 (**Fig. 5c**). Hence, the bivalent binding also leads to extended residence time compared to monovalent ligands.

We next studied the disruption of BRD4 foci in native U2OS cells. We observed bright BRD4 foci with immuno-staining using an anti-BRD4 antibody (**Fig. 6a**) and confirmed the specificity of the antibody by siRNA knockdown of BRD4. Recent literature has described asymmetrical loading of BRD4 to super-enhancers (SEs), which are often associated with key genes that determine cell fate or those involved in oncogenesis[27,28]. Histone H3K27 acetylation is a marker for active enhancers[29]. Mediator complex subunit 1 (MED1) and BRD4 have previously been shown high levels of binding to SEs and their levels are strongly correlated throughout the genome[30]. Consistent with this, immuno-costaining experiments showed that MED1 and H3K27Ac form foci in U2OS cells which overlap completely with those of BRD4.

Treatment with **6** at 10 nM led to complete disruption of BRD4 and MED1 foci (**Fig. 6b**). Concentration-response data for **1** and **6** in this assay showed that **6** was a signficantly more potent inhibitor (pIC_{50} 7.4 and 10 for **1** and **6** respectively, **Supplementary Fig. 11**). There was no apparent change of H3K27Ac foci up to 24 h treatment with BRD4 inhibitors, whereas the disruption of BRD4 and MED1 foci reached maxima within 3-4 h.

The enhanced potency of **6** in BRD4 related assays translated into cancer cell killing activity in a mixed panel of heamatoloical cell lines (**Fig. 6c** and **Supplementary Fig. 12**). The bivalent binding of **6** translated into highly potent cell killing activity in BRD4-dependent cell lines (pIC_{50} of 9.5 in both MV4.11 and MM.1S lines), representing a potency increase of approximately 3 orders of magnitude compared to **1**. Activity against BRD4 independent K-562 cells was weaker than for sensitive lines with both **1** and **6**. Interestingly, the ALL cell line RS4-11 was quite sensitive to both BET inhibitors. However, monovalent **1** failed to achieve full inhibition, even at higher concentrations, whereas bivalent **6** still achieveed near complete cell killing. This provides evidence of differentiated and possibly advantageous pharmacology from bivalent inhibition. Changes in gene expression in response to treatment with **1** and **6** in MM.1S, MV-4-11 and K-562 cells revealed very similar expression profiles in response to both inhibitors (see Online Methods section) suggesting that enhanced cell killing effects of **6** are a direct consequence of the increased inhibitory potency as a result of bivalent inhibition rather than altered downstream gene expression.

To further corroborate the extended intracellular BRD4 residence time observed for **6**, we performed a drug washout using MM.1S cells and monitored c-Myc protein recovery overtime (**Fig. 6d**). This clearly showed that **6** maintains knockdown of c-Myc protein levels upto 16 hours post washout. In contrast, upon treatment with **1**, c-Myc levels return to control levels within 1 hour of washout.

Discussion

This study revealed unique BET inhibitors (biBETs), which simultaneously engage two bromodomains leading to biochemical and cellular consequences beyond those shown with monovalent inhibitors. Enhanced cell potency correlated across a range of cell formats and end-points including AR and ERα

immuno fluorescence in prostate and breast cancer cells respectively, transiently expressed engineered BRET protein-protein interaction systems and well characterised BRD4 related end-points such as c-Myc DR in leukaemia cells (**Supplementary Table 7**). The level of potency and selectivity achieved by **6**, coupled with the comprehensive evidence for its enagement with BRD4 in cells make it the best cellular probe to date when judged against recently described criteria for chemical probes.[31]

The results we have described provide compelling evidence for the bivalent mechanism. The cellular SAR for the analogues is highly suggestive of **6** binding two BRDs simultaneously. The X-ray crystal structures of the compounds in complex with an isolated BRD4(1) construct clearly demonstrate their ability to induce dimerisation of two BRDs. The NMR experiments on tandem domain constructs showed that **6** engages both BRD4 BD1 and BD2 simultaneously in solution. The AUC data demonstrated that binding of **6** leads to a protein of smaller radius than either the apo protein or that in complex with a monovalent ligand, suggesting that the bound complex in solution is mostly monomeric with respect to protein and that compound binding induces a more compact structure. SAXS experiments showed a folding of the protein in response to ligand binding and demonstrate that the complex with **6** brings the two BRDs into close proximity, similar to that observed in the X-ray structures of BRD4(1) dimer. Together, these data provide strong evidence for the formation of significant populations of *in cis* complex under the conditions studied. The dramatic increase in potency observed in the cellular NanoBRET experiment for displacement of BRD4(1,2) from acetylated histone, relative to the BD1 construct alone, the analogous loss in BRD4(1,2) binding potency with the BRD4(2) binding site blocking mutation (N433F) and subsequent translation of this increased potency into BRD4 driven pharmacology, along with increased BRET response for binding to doubly tagged BRD4(1,2) provide very strong evidence that **6** binds bivalently in cells with a significant population of an *in cis* complex forming.

Cellular growth inhibition data showed that differential and potentially advantageous pharmacology arises from the bivalent binding mode in that complete inhibition of less sensitive cell lines was observed with **6**, whereas monovalent ligands failed to achieve complete inhibition in these settings. This may be a result of bivalent binding *per se* or as a follow on consequence of the slow dissociation arising from the bivalent mechanism. We anticipate that these effects will translate to *in vivo* settings although this would require optimization of pharmacokinetic profiles. The pharmacology of bivalent inhibitors with optimized *in vivo* exposure are the subject of further publications[32,33].

The increased potency due to bivalent binding is presumably an avidity effect[34]. Previous attempts to produce bivalent binders to BRDs[35,36] and other proteins[37] have been attempted in the past by linking two separate small molecule ligands with a flexible linker. Compounds such as biBET-6 ,which partially fuse the two binding elements results in much more physical properties (**6** has molecular weight of 531 and $\log D_{7.4}$ of 2.9), thus these compounds could conceivably be optimised to drugs. Many proteins possess an arrangement of ordered functional domains joined by extended disordered regions. In particular, in the epigenetics field, protein-histone interactions achieve their affinity and specificity through the sum of weak interactions with different epigenetic marks[38,39,40,41]. Development of bivalent ligands for these proteins in a manner analogous to that described here, could provide a means of developing superior chemical probes and, ultimately, drug molecules (**Supplementary Fig. 14a**) and could also provide a more effective means of targeting protein:protein complexes (**Supplementary Fig. 14b**) (for further discussion, see Supplementary Note 2).

From an initial hit molecule with an unknown target, we were able to follow cellular SAR to elucidate its molecular mechanism. Further optimisation of the compounds based on this mechanistic hypothesis substantially improved potency by structure-based design, increasing the potency from micromolar to picomolar as a consequence of bivalent target engagement. As a result, we have created biBET ligands which can simultaneously bind to two bromodomains. It is also notable that these bivalent molecules deliver a very substantial increase in potency while maintaining acceptable size and physical properties. The resulting compound, biBET-6, is a very potent, selective inhibitors of BET BRDs and provides a

chemical probe with distinct advantages over those previously described. We anticipate that this will be invaluable in further elucidating the complex biology of BET proteins.

Accession codes

Pdb codes: 5ad2 for BRD4(1) in complex with **2**, 5ad3 for BRD4(1) in complex with **6**.

Acknowledgements

The authors would like to thank Greg Carr, Scott Lamont, Tom Moss, Anil Patel and Gail Wrigley for the synthesis of test compounds; Helen Ashton for co-ordinating biological testing at DiscoverX, Kay Eckersley and Paula McArdle for supporting cellular imaging studies and Panagis Filippakopoulos for BRD4 mutant vector constructs. We thank Kevin Embrey for helpful comments on the compilation of the manuscript.

Author Contributions

M.J.W. designed compounds, coordinated chemistry, analysed and interpreted data and coordinated manuscript preparation. H.C. coordinated cell biology work and analysed and interpreted biological and biophysical data. A.A.R. designed compounds, carried out computational modeling and structural analysis and interpreted data. G.W. coordinated biophysical testing and AR / ER based cell experiments and conceived of and coordinated nanoBRET experiments. R.B. designed and carried out of NMR studies. S.B. carried out cell biology experiments. R.H.B. designed compounds, coordinated of chemistry and analysed and interpreted data. R.C. carried out ER cell biology experiments. E.C. was the project leader. I.D. carried out NanoBRET experiments. D.L.D. coordinated NanoBRET target engagement experiments and construct production. A. D. coordinated transciptomic profiling and interpreted data. L.F. designed, expressed and purified protein constructs. G.H. analysed and interpreted biophysical data. T.A.J. carried out AUC experiments and *ab initio* modeling. A.K. carried out SAXS experiments. M.McM. coordinated AUC experiments and analysed and interpreted biophysical data. J.M. conducted NanoBRET target engagement experiments. D.O. coordinated SAXS experiments and analysed and interpreted biophysical data. J.P. carried out protein x-ray structure determination. P.P. carried out the c-Myc flow cell assay. G.R.R. carried out computational modeling of tandem domain proteins. M.B.R. carried out NanoBRET target engagement experiments. S.S. carried out transcriptomics experments. N.S. carried out AR cell biology experiments. D.I.S. coordinated and carried out SAXS experiments. W.W. carried out cell biology experiments. D.W. synthesised compounds. D.M.W. analysed and interpreted the data. Y.Y. carried out transcriptomics experiments. All authors discussed results and commented on the manuscript.

References

1. Vidler, L.R., Brown, N., Knapp, S. & Hoelder, S. Druggability and structural classification of bromodomain acetyl-lysine sites. *J. Med. Chem.* **55**, 7346-7359 (2012).
2. Prinjha, R.K., Witherington, J. & Lee, K. Place your BETs: the therapeutic potential of bromodomains. *Trends Pharmacol. Sci.***33**, 146-153 (2012).
3. Nicodeme, E. *et al*. Supression of inflammation by a synthetic histone mimic. *Nature* **468**, 1119-1123 (2010).
4. Mirguet, O. *et al.* Discovery of epigenetic regulator I-BET762: lead optimization to afford a clinical candidate inhibitor of the BET bromodomains. *J. Med. Chem*. **56**, 7501-7515 (2013).
5. Filippakopoulos, P. *et al.* Selective inhibition of BET bromodomains. *Nature* **468**, 1067-1073 (2010).
6. Wu, S.-Y. & Chiang, C.-M. The double bromodomain-containing chromatin adaptor Brd4 and transcriptional regulation. *J. Biol. Chem*. **282**, 13141-13145 (2007).
7. Vollmuth, F., Blankenfeldt, W. & Geyer, M. Structures of the dual bromodomains of the P-TEFb-activating protein Brd4 at atomic resolution. *J. Biol. Chem*. **284**, 36547-36556 (2009).

8. Delmore, J. E. *et al*. BET bromodomain inhibition as a therapeutic strategy to target c-Myc. *Cell* **146**, 904-917 (2011).
9. Dawson, M. A. *et al*. Inhibition of BET recruitment to chromatin as an effective treatment for MLL-fusion leukaemia. *Nature* **478**, 529-533 (2011).
10. Stathis, A. *et al*. 5LBA Results of a first-in-man phase I trial assessing OTX015, an orally available BET-bromodomain (BRD) inhibitor, in advanced hematologic malignancies. *Eur. J. Cancer* **50**, 196 (2014).
11. Bradbury, R. H. *et al*. Discovery of AZD3514, a small-molecule androgen receptor downregulator for treatment of advanced prostate cancer. *Bioorg. Med. Chem. Lett*. **23**, 1945-1948 (2013).
12. Loddick, S.A. *et al*. AZD3514: a small molecule that modulates androgen receptor signaling and function *in vitro* and *in vivo. Mol. Cancer Ther.* **12**, 1715-1727 (2013).
13. Quinn, E. *et al*. BROMOscan - a high throughput, quantitative ligand binding platform identifies best-in-class bromodomain inhibitors from a screen of mature compounds targeting other protein classes. *Cancer Res*. 73, Supplement 4238-4238 (2013).
14. Morris, J. et al. NCI-60 response profiles of >400 investigational oncology agents: a resource enabling drug and biomarker discovery. *Mol Cancer. Ther.* **12**, A102 (2013).
15. Morris, J. *et al*. 5475: Interrogation of NCI-60 patterns of growth inhibition in conjunction with investigational oncology agents kinase profiling for the elucidation of mechanistic targets. *Cancer Res*. **74**, 5475 (2014).
16. Asangani, I. *et al.* Therapeutic targeting of BET bromodomain proteins in castration-resistant prostate cancer. *Nature* **510,** 278-282 (2014).
17. Feng, Q. *et al*. An epigenomic approach to therapy for tamoxifen-resistant breast cancer. *Cell Res.* **24**, 809–819 (2014).
18. Williams, F. P. *et al.* Segmental isotope labelling of an individual bromodomain of a tandem domain BRD4 using sortase A. PLoS One, DOI: 10.1371/journal.pone.0154607 (2016).
19. Ledowitz, J., Lewis, M.S. & Schuck, P. Modern analytical ultracentrifugation in protein science: a tutorial review. *Protein Sci*. **11**, 2067-2079 (2002).
20. Brown, P.H. & Schuck P. *Biophys. J.* Macromolecular size and shape distributions by sedimentation velocity analytical ultracentrifugation. *Biophys J.* **90**, 4651–4661 (2006).
21. Mertens, H.D., Svergun, D.I. Structural characterization of proteins and complexes using small-angle X-ray solution scattering. *J. Struct Biol*. **172**, 128-141 (2010).
22. Tria, G., Mertens, H.D., Kachala, M. & Svergun, D.I. Advanced ensemble modelling of flexible macromolecules using X-ray solution scattering. *IUCrJ*. **2**, 207-217 (2015).
23. Machleidt, T. *et al*. NanoBRET—A Novel BRET platform for the analysis of protein–protein interactions. *ACS Chem.Biol*. DOI:10.1021/acschembio.5b00143 (2015).
24. Baud, M. G. *et al.* Chemical biology. A bump-and-hole approach to engineer controlled selectivity of BET bromodomain chemical probes. *Science* **346**, 638-641 (2014).
25. Philpott, M. *et al*. Assessing cellular efficacy of bromodomain inhibitors using fluorescence recovery after photobleaching. *Epigenetics Chromatin* 7, 14-25 (2014).
26. Robers, M.B. *et al*. Target engagement and drug target residence time can be measured in living cells with BRET. *Nat. Commun*. **6**, 10091 (2015).
27. Whyte, W.A. *et al*. Master transcription factors and mediator establish super-enhancers at key cell identity genes. *Cell* **153**, 307–319 (2013).
28. Hnisz, D. *et al*. Super-enhancers in the control of cell identity and disease. *Cell* **155**, 934–947 (2013).
29. Creyghton, M.P. *et al*. Histone H3K27ac separates active from poised enhancers and predicts developmental state. *Proc. Nat. Acad. Sci*. **107**, 21931-21936 (2010).
30. Lovén, J. *et al.* Selective inhibition of tumour oncogenes by disruption of super-enhancers. *Cell* **153**, 320-334 (2013).

31. Arrowsmith, C.H. *et al*. The promise and peril of chemical probes. *Nature Chem. Biol*. **11**, 536-541 (2015).
32. Waring, M. J. *et al*. Optimisation of a series of bivalent triazolopyridazine based BET bromodomain inhibitors: the discovery of (3R)-4-[2-[4-[1-(3-methoxy-[1,2,4]triazolo[4,3-b]pyridazin-6-yl)-4-piperidyl]phenoxy]ethyl]-1,3-dimethyl-piperazin-2-one, AZD5153, *J. Med. Chem.* DOI/10.1021/acs.jmedchem.6b00070 (2016).
33. Chen, H. *et al.* AZD5153: a novel bivalent BET bromodomain inhibitor highly active against hematologic malignancies, *Mol. Cancer Ther*. in press (2016).
34. Krishnamurthy, V.M., Estroff, L.A. & Whitesides, G.M. Ch. 2 Multivalency in ligand design in Fragment-based approaches in drug discovery, Jahnke, W. & Erlanson, D.A. Eds. (Wiley, Weinheim, Germany, 2006).
35. Arnold, D.L., Foreman, K.W., Jin, M., Wanner, J. & Werner, D.S. Preparation of bivalent bromodomain ligands for treating a disease associated with a protein having tandem bromodomains. PCT Int. Appl. WO 2013033268 (2013).
36. Arnold, D.L., Foreman, K.W. & Werner, D.S. Preparation of bivalent bromodomain ligands, and methods of using the same. PCT Int. Appl. WO 2015081284 (2015).
37. Sun, H. *et al*. Design, synthesis, and characterization of a potent, nonpeptide, cell-permeable, bivalent Smac mimetic that concurrently targets both the BIR2 and BIR3 domains in XIAP, *J. Am. Chem. Soc.* **129**, 15279-15294 (2007).
38. Jacobson, R.H., Ladurner, A.G., King, D.S. & Tijan, R. Structure and function of a human $TAF_{II}250$ double bromodomain module. *Science*, **266**, 1422-1425 (2000).
39. Ruthenburg, A.J., Li, H., Patel, D.J., Allis, C.D. Multivalent engagement of chromatin modifications by linked binding modules. *Nat. Rev. Mol. Cell. Bio*. **8**, 983-993 (2007).
40. Morinière, J. *et al*. Cooperative binding of two acetylation marks on a histone tail by a single bromodomain. *Nature*, **461**, 664-668 (2009).
41. Ruthenburg, A.J. *et al*. Recognition of a mononucleosomal histone modification pattern by BPTF via multivalent interactions. *Cell*, **145**, 692-706 (2011).

Figure Legends

Fig. 1 – Discovery of a novel class of BRD inhibitor. a) Prototypic BET inhibitor i-BET762 (**1**) and potent AR down regulator **2**. b) BRD selectivity data for **2** showing % binding at 10 μM, numbers above bars denote pK_d values. c) Concentration response for c-Myc DR by Western blotting for **1** and **2** in MM.1S cells (for further details see Online Methods section).

Fig. 2 – X-ray crystal structure of **2** bound to BRD4(1) (pdb code 5AD2). a) Compound induced dimerisation. b) Interactions made by the TPDZ group in the acetyl lysine pocket. c) Interactions made by the piperazinone in the second acetyl lysine pocket. Hydrogen bond distances (green dotted lines) are shown.

Fig. 3 - Cellular SAR and optimisation of bivalent binding leading to **6**. a) Deletions of BRD binding elements. b) Optimised bis-TPDZs **6** and **7** and an inactive control compound **8** modified to abrogate both binding events. c) Concentration response overlays for **6** in Bromoscan competition binding assays for BRD4(1) (circle), BRD4(2) (square) or BRD4(1,2) (triangle) d) X-ray structure of BRD4(1) dimer induced by **6** (pdb code 5AD3) (**Supplementary Table 4**).

Fig. 4 – Biophysical characterisation of bivalent binding. a) 2D ^{1}H-^{15}N TROSY HSQC spectra recorded at 18.8 T of U-[^{2}H,^{15}N]-labeled BRD4(44-460)(grey) comapred to the spectra in the presence of **1** (red) and **6** (blue) at a ligand to protein ratio of 2:1. Boxed regions are shown expanded in **Supplementary Fig. 7c** and correspond to (i) a BD1 residue (unassigned) and (ii) the W374 indole amine of BD2. b) Sedimentation coefficient distributions for apo-BRD4(1-477) (grey) and in the presence of **1** (red) and **6** (blue at 1:1 and 2:1 ligand:protein ratios. c) Sedimentation coefficient distributions for **6** at 1:1 overlaid with the contour heat map of likely frictional ratios across the peaks. d) *Ab initio* shapes of the BRD4 constructs restored from the SAXS data for apo-BRD4 (grey) and 1:1 complexes of **1** (red) and **6** (blue); mean (± standard deviation). Further data on interdomain

distances, R_g values derived from model fitting and χ^2 values showing the goodness of the fit are given in **Supplementary Table 6**.

Fig. 5 – Characterisation of binding mode in cells using nanoBRET systems. a) NanoBRET concentration response curves for displacement of BRD4(1), full-length BRD4 and BRD4(N433F) from labeled histone H3.3-Halo-tag by **1** and **6** comparing BRD4(1) to full length BRD4 in HCT116 cells (top) and full length BRD4(1) to BRD4(N433F) in HEK293 cells (bottom), data are means of 3 independent determinations and the error bars show the standard error in the means. b) NanoBRET system containing BRD4(1,2) with HaloTag BRD4(1) and NanoLuc BRD4(2) showing increased BRET response for WT BRD4(1,2) in the presence of **6**, not observed for the N140F mutant or for binding of **1**, data are means of 3 independent determinations and the error bars show the standard error in the means. c) Intracellular NanoBRET target engagement using a fluorescent iBET-762-based tracer. Competitive displacement from full-length BRD4, BRD4(N433F) and BRD4 (1) in HeLa cells by **1** and **6**. Residence time analysis of Compounds **1** and **6** on BRD4(1), full length BRD4 and BRD4(N433F) in HeLa cells, data are means of 3 independent determinations and the error bars show the standard error in the means.

Fig. 6 – Potency in cellular assays of BRD4 pharmacology. a) Formation of bright foci from super-loading of BRD4 or Med1 to the super-enhancers (SE) marked by histone H3K27Ac in the chromatin regions. b) Disruption of BRD4 and Med1 foci by **6** (10 nM) and concentration response data for **1** and **6**. c) Growth inhibition data for 1 and **6** in BRD4 sensitive and insensitive lines. Curves illustrate the responses in a sensitive (MM.1S) and less sensitive (RS411) line. Full curves for the other tested lines are shown in **Supplementary Fig. 12**. d) c-Myc protein levels measured by Western blots for **1** (1 μM) and **6** (50 nM) compared to DMSO control at 2, 4 and 16 hours post compound washout in MM.1S cells (for full length gels see **Supplementary Fig. 13**), error bars represent the standard deviations of triplicate determinations.

Online Methods

In vitro ADME data for 6

Data were generated using standard protocols[42,43].

Protein preparation

Plasmid constructs

Variants of human BRD4 were generated by gene synthesis with an N-terminal hexahistidine tag and tobacco etch virus (TEV) protease site, and subcloned into pET28 vector for E.coli expression.

BRD4(1,2) (residues 1-477), BRD4(1,2) (residues 44-460), BRD4(1) (residues 42-169), BRD4(2) (residues 333-460).

Protein expression

In E. coli cells (BL21-Gold (DE3); Novagen), BRD4 proteins were induced using 0.1 mM isopropyl-β-D-1-thiogalactopyranoside (IPTG) overnight at 18 °C.

Protein purification

Cells were resuspended in 50mM Tris pH 8.0, 300mM NaCl, 1mM β-mercaptoethanol, 10mM Imidazole containing Complete protease inhibitor tablets (Roche) and Benzonase nuclease

(2.5u/ml).Resuspended cells were lysed using a Constant Systems cell disruptor at 25kpsi and clarified by centrifugation at 75,000 xg for 2 hours at 4ºC.

BRD4 was purified from the supernatant by Nickel affinity chromatography, followed by cation exchange chromatography. Protein was further purified by size exclusion chromatography using a Superdex 75 10/300 GL column in 20mM Hepes pH 7.4, 100mM NaCl, 1mM Tris(2-carboxyethyl) phosphine hydrochloride.

For NMR spectroscopy and X-ray crystallography,the hexahistidine tag was removed from BRD4 by treatment with TEV protease after the Nickel affinity chromatography.

Crystallisation & Structure of BRD4(1) in complex with 2

E.coli expressed BRD4-(42-169) at a concentration of 10mg/ml was mixed with **2** to a final concentration of 200 µM, 2% DMSO and incubated on ice for 1 hour. Note that due to limited solubility and DMSO tolerance, a molar excess of the compound concentration could not be attained. Low volume sitting drop crystallisation was performed in MRC 2 well plates using a ratio of 2:1 protein : mother liquor and crystals formed in a condition containing 0.2M NaCl, 5.9% PEG 3350 (w/v), 10% ethylene glycol, 0.1M Hepes pH 7.4 at 4 °C. Crystals were cryoprotected in mother liquor supplemented with a further 20% ethylene glycol. Diffraction data was collected using a Rigaku FRE superbright generator with Osmic mirrors and a Saturn 944 CCD detector and processed using XDS[44]. Molecular replacement solution was determined with 2OSS.pdb using Phaser[45]. The $P2_12_12_1$ cell ($\alpha=\beta=\gamma=90°$, a=41.618Å, b=59.615Å, c=106.773Å) has a dimer in the ASU. Model building was performed using Coot[46] and refined using Buster[47]. **2** could easily be modelled into the difference density using ligand restraints generated by Grade[48]. It should be noted that the electron density for the ligand was of sufficient quality to enable it to be built in two alternate and equivalent conformations with a total final occupancy of 1.0. The statistics for the data collection and refined co-ordinates are given in (**Supplementary Table 1**). The final model has been deposited in the protein databank under accession code 5ad2.

Crystallisation & Structure of BRD4(1) in complex with 6

E.coli expressed BRD4-(42-169) at a concentration of 10mg/ml was mixed with **6** to a final concentration of 200 µM, 2% DMSO and incubated on ice for 1 hour. Note that due to limited solubility and DMSO tolerance, a molar excess of the compound concentration could not be attained. Low volume sitting drop crystallisation was performed in MRC 2 well plates using a ratio of 2:1 protein : mother liquor and crystals formed in a condition containing 0.2M $(NH_4)_2HPO_4$, 20% PEG 3350 (w/v) at 4 °C. Crystals were cryoprotected in mother liquor supplemented with a further 20% ethylene glycol. Diffraction data was collected at beamline IMCA-CAT 17ID, Advanced Photon Source, Argonne National Laboratory, USA using a Dectris Pilatus 6M Pixel Array detector and processed using XDS. Molecular replacement solution was determined with 2OSS.pdb using Phaser. The $P2_12_12_1$ cell ($\alpha=\beta=\gamma=90°$, a=109.64Å, b=41.826Å, c=59.591Å) has a dimer in the ASU. Model building was performed using Coot and refined using Buster. **6** could easily be modelled into the difference density bound in a single orientation at occupancy of 1.0 using ligand restraints generated by Grade. The statistics for the data collection and refined co-ordinates are given in (**Supplementary Table 5**). The final model has been deposited in the protein databank under accession code 5ad3.

Measurement of endogenous ERα levels in the MCF-7 cell line

Measurement of endogenous ERα levels in the MCF-7 cell line was carried out as previously described[49]. Briefly, the MCF-7 human breast ductal carcinoma cell line from the American Type Culture Collection (ATCC; HTB-22) was revived directly from a cryovial in phenol red free Dulbecco's Modified Eagle's medium (DMEM) containing 2 mM L-glutamine and 5% (v/v) charcoal/dextran treated foetal calf serum (FCS). Cells were seeded into black,

transparent bottomed, 384-well plates, at 1500 cells per well in a volume of 40 µl using a Multidrop Combi dispenser (Thermo Scientific). Cell plates were incubated for 24 hrs at 37 °C, 5% CO_2. An Echo 555 acoustic dispenser was used to dispense test compounds directly into cell plates producing a 12 point half-log duplicate concentration range (3.125 µM top concentration). DMSO was dispensed in the maximum signal control wells to give a final concentration of 0.3% (v/v) and fulvestrant was dispensed in the minimum signal control wells to give a final concentration of 100 nM. Cells were incubated for 18-24 hrs at 37 °C, 5% CO_2 and then fixed using a 3.7% (v/v) final formaldehyde concentration for 20 minutes. The cells were washed three times with 250 µl phosphate buffered saline solution (PBS) using a BioTek ELx405 plate washer (BioTek Instruments, UK), and 50 µl of PBS was added to all wells. The PBS was aspirated and the cells permeabilised with 40 µl PBS containing 0.5% (v/v) Tween 20 for 1 hr at room temperature. The cells were then washed three times in 250 µl of PBS / 0.05% (v/v) Tween 20 (PBST) using a BioTek EL406 plate washer. 20 µl was added per well of a 1:1000 dilution of ERα (Clone SP1 (epitope contained within a synthetic peptide derived from C-terminal of human estrogen receptor)) monoclonal rabbit antibody (Thermo Scientific, #RM-9101-S) in PBST / 3% (w/v) bovine serum albumin (BSA) and the plates were incubated overnight at 4 °C. The cells were washed three times in 250 µl of PBST and then incubated with 20 µl per well of a 1:500 dilution of goat anti-rabbit IgG Alexa Fluor 594 (Molecular Probes, Life Technologies, Paisley, UK) and a 1:5000 dilution of Hoechst (Molecular Probes) in PBST / 3% (w/v) BSA for 1 hr at room temperature. The cells were washed three times in 250 µl of PBST, 40 µl of PBS was then added per well, and the plates covered with a black plate seal. Cell images were acquired using a Cellomics Arrayscan VTI HCS reader (Thermo Scientific) using a 10 x 0.3NA objective and applying the filters BGFR_386_23 and BGFR_549_15 to detect Hoechst and Alexa Fluor 594 signals. Using the Compartmental Analysis v4 bio-application nuclear masks were generated from the Hoechst stained nuclei in channel 1 and a suitable threshold was applied in channel 2 to quantify ERα within the nuclear masks. The mean total intensity was normalized for cell number giving the total intensity of ERα staining per cell.

Measurement of endogenous AR levels in the LNCaP cell line

(A) 96 well method using mouse anti-human AR monoclonal antibody (clone AR441).

A modification of the previous immunofluorescence end point assay[11] was used to measure levels of nuclear AR in the LNCaP prostate carcinoma cell line [LNCaP clone FGC (CRL-1740) obtained from the American Type Culture Collection (ATCC)]. LNCaP cells were cultured in Growth Medium [phenol red free Roswell Park Memorial Institute (RPMI) 1640 (Invitrogen Code no. 11835-063), containing 2 mM L-Glutamine (Invitrogen Code no. 25030-024) and 1%(v/v) Penicillin/Streptomycin (10000 units/ml Penicillin and 10000 µg/mL of Streptomycin utilising penicillin G sodium salt) and streptomycin sulphate (prepared in normal saline, Invitrogen Code no. 15140122) and 10%(v/v) foetal bovine serum (FBS)] in a 5% CO_2 air incubator at 37ºC. Cells for assay were harvested from T175 stock flasks by washing once in PBS (phosphate buffered saline, pH 7.4) (Invitrogen Code no. 14190-094) and harvested using 5 mL of 1 x Trypsin / ethylaminediaminetetraacetic acid (EDTA) (10 x Trypsin-EDTA, 5.0 g/L Trypsin, 2.0 g/L of EDTA•4Na and 8.5 g/L of NaCl, without Phenol Red, Invitrogen Code no. 15400-054) diluted in PBS solution. A 5 mLvolume of Assay Medium was then added to each flask [as above except that 5% (v/v) charcoal stripped FBS (HyClone Code no. SH30068.03) was included instead of 10% (v/v) FBS]. Cells were syringed at least twice using a sterile 18G x 1.5" (1.2 x 40 mm) broad gauge needle and cell density was measured using a Countess automated cell counter (Life Technologies). Cells were further diluted in Growth Medium plus 5% (v/v) charcoal stripped FBS and seeded at a density of $6.5x10^3$ cells per well (in 90 µL) into transparent , black, tissue culture treated 96-well plates (Corning, # 3904). Plates were incubated overnight at 37°C, 5% CO_2. A 10x compound dose response plate with DMSO normalised to 3% (v/v) was generated in 30 µL of assay media using the Labcyte Echo 555 acoustic dispenser and a 10 µL volume of diluted compound was then dosed to cells using a Thermo Scientific Matrix PlateMate to give a final

concentration of 0.3% (v/v) DMSO and 8 or 12 point half-log singlicate concentration range (30 μM or 3 μM top concentration). DMSO was dispensed in the maximum signal control wells to give a final concentration of 0.3% (v/v) and either AZ13182659 or **6** was dispensed to generate a minimum signal to give a final concentration of 30μM or 3μM, respectively. Plates were then further incubated for 20-22 hours at 37°C, 5% CO_2. Plates were then fixed by the addition of 20 μL of 10% (v/v) formaldehyde solution (in PBS) to each well [final formaldehyde concentration = 1.67%(v/v)] and left at room temperature for 10 min. The fixative solution was removed and cells were washed three times with 250 μL of PBS/0.05% (v/v) Tween 20 (PBST) using a Tecan PW96 plate washer (Tecan UK) and 50 μl of PBS was added to all wells. Immunostaining was performed at room temperature. Cells were permeabilised by the addition of 35 μL of PBS containing 0.5% (v/v) Tween 20 and incubated for 1 h at room temperature. Permeabilisation solution was removed and cells were washed three times with 250 μL of PBST using an automated plate washer. 35 μL of Blocking Solution [PBST containing 3% (w/v) Marvel dried skimmed milk (Nestle)] was added to each well and plates were incubated at room temperature for a minimum of 1 h. Following removal of the Blocking Solution with a plate washer, 35 μL of mouse anti-human AR monoclonal antibody (clone AR441, DAKO, Code No. M3562), diluted 1:500 in Blocking Solution, was added to each well and incubated for 1 h.
The primary antibody solution was removed from the wells followed by 3 x 100 μL PBST washes using a plate washer. Then 35 μL of Alexa-Fluor 488 goat anti-mouse IgG secondary antibody (Invitrogen, Code No. A-11001), diluted 1:500 and Hoechst (Molecular Probes), diluted 1:5000 in Blocking Solution, was added to each well. Henceforth, wherever possible, plates were protected from light exposure. The plates were incubated for 1 h and then the secondary antibody solution was removed from the wells followed by 3 x 100 μL PBST washes using a plate washer. Then 50 μL of PBST was added to each well and plates were covered with a black plate seal. Cell images were acquired using a Cellomics Cell Insight reader (Thermo Scientific) using a 10 x 0.3NA objective and applying the filters BGRFR_386_23 and BGRFR_485_20 to detect Hoechst and Alexa Fluor 488 signals. Using the Compartmental Analysis v4 bio-application nuclear masks were generated from the Hoechst stained nuclei in channel 1 and a suitable threshold was applied in channel 2 to quantify AR within the nuclear masks. The mean total intensity was normalized for cell number giving the total intensity of AR staining per cell. Sample Images are detailed in **Supplementary Fig. 15**.

(B) 384 well method using rabbit anti-human AR monoclonal antibody (PG-21)

LNCaP cells were cultured as described above. Cells were seeded into black, clear bottom, 384-well plates (Costar # 3712) at 3000 cells per well in a volume of 40 μl using a Multidrop Combi dispenser (Thermo Scientific) and then incubated overnight at 37°C, 5% CO_2. An Echo 555 acoustic dispenser was used to dispense test compounds directly into cell plates producing a 12 point half-log singlicate concentration range (30 μM or 3 μM top concentration). Minimum and maximum controls were the same as for the 96 well assay. Plates were then further incubated with compound for 18 hours at 37°C, 5% CO_2. Cells were fixed by addition of 20μl/well of 12%(v/v) formaldehyde using a Thermo Scientific Matrix WellMate liquid handler (final formaldehyde concentration 4%(v/v)) and plates incubated at room temperature for 20 minutes. The fixative solution was removed and cells were washed once with 250 μL of PBS/0.05% (v/v) Tween 20 (PBST) using a using BioTek ELx405 plate washer (BioTek Instruments, UK). Cells were then permeabilised by adding 20μl/well PBS containing 0.1% Triton X-100 and incubated for 20 min at room temperature. Cells were washed once in PBS. Next, 20μl/well of PG-21 primary antibody (MilliPore #06-680) diluted 1:400 in antibody buffer (PBS/Tween 0.05% + 5% FCS), was added per well and plates incubated overnight at 4ºC. The following day, the plates were washed three times with PBS prior to addition of 20μl/well of secondary antibody (goat anti-rabbit AlexaFluor 488 diluted 1:500 in antibody buffer plus Hoechst nuclear stain diluted 1:5000). Plates were protected from light and incubated for one hour at room temperature. The plates were then washed 3 times in PBS without a final aspiration step and covered with black plate seals. Cell images were acquired as above for the AR441 method. Sample Images are detailed in **Supplementary Fig. 16**.

Data analysis

During the routine running of the biochemical and cellular cascade experimental data from each of the assays was exported into Genedata Screener® client graphing software (Genedata AG, Basel, Switzerland) to perform curve fitting analysis. For the representative curves exemplified in the figures the data was plotted using Prism software (GraphPad Prism 6 Software, La Jolla, CA). A nonlinear regression curve fit using four-parameters with variable slope was applied.
IC_{50} values were determined by calculation of the concentration of test compound that was required to give a 50% reduction of the total measured effect corrected for background (average maximum control value minus the average minimum control value). The quality of each assay was determined by analysis of the Z' factor[50].

Measurement of AR binding

Binding to AR was measured in LNCaP cellular extracts following an established method[51].

Bromoscan™ profiling

Technology Overview - BROMO*scan*™ is a technology platform for identifying small molecule bromodomain inhibitors. Based on proven KINOME*scan*™ technology, BROMO*scan*™ employs a proprietary ligand binding site-directed competition assay to quantitatively measure interactions between test compounds and bromodomains. This robust and reliable assay panel is suitable for high throughput screening and delivers quantitative ligand binding data to facilitate the identification and optimization of potent and selective small molecule bromodomain inhibitors. BROMO*scan*™ assays include trace bromodomain concentrations (<0.1 nM) and thereby report true thermodynamic inhibitor K_d values over a broad range of affinities (<0.1 nM to >10 µM).

BROMO*scan* Primary Screen Protocol

T7 phage strains displaying bromodomains were grown in parallel in 24-well blocks in an *E. coli* host derived from the BL21 strain. *E. coli* were grown to log-phase and infected with T7 phage from a frozen stock (multiplicity of infection = 0.4) and incubated with shaking at 32°C until lysis (90-150 minutes). The lysates were centrifuged (5,000 x g) and filtered (0.2µm) to remove cell debris. Streptavidin-coated magnetic beads were treated with biotinylated small molecule or acetylated peptide ligands for 30 minutes at room temperature to generate affinity resins for bromodomain assays. The liganded beads were blocked with excess biotin and washed with blocking buffer (SeaBlock (Pierce), 1 % BSA, 0.05 % Tween 20, 1 mM DTT) to remove unbound ligand and to reduce non-specific phage binding. Binding reactions were assembled by combining bromodomains, liganded affinity beads, and test compounds in 1x binding buffer (16 % SeaBlock, 0.5x PBS, 0.02%BSA, 0.04 % Tween 20, 0.004% Sodium azide, 7.9 mM DTT). Test compounds were prepared as 1000X stocks in 100% DMSO and subsequently diluted 1:25 in monoethylene glycol (MEG). The compounds were then diluted directly into the assays such that the final concentrations of DMSO and MEG were 0.1% and 2.4%, respectively. In the primary screen compounds were tested at a final concentration of 3µM. All reactions were performed in polypropylene 384-well plates in a final volume of 0.02 ml. The assay plates were incubated at room temperature with shaking for 1 hour and the affinity beads were washed with PBST (1x PBS, 0.05% Tween 20). The beads were then re-suspended in elution buffer (1x PBS, 0.05% Tween 20, 2 µM non-biotinylated affinity ligand) and incubated at room temperature with shaking for 30 minutes. The bromodomain concentration in the eluates was measured by qPCR.

BROMO*scan* K_d Protocol

This was carried out as for the primary screen protocol above except for compound handling. An 11-point 3-fold serial dilution of each test compound was prepared in 100% DMSO at 1000x final test concentration. This serial is then diluted to 100x in ethylene glycol and subsequently diluted to 1x in the assay (final DMSO concentration = 0.1%, Ethylene glycol concentration=0.9%). K_ds were

determined using a compound top concentration = 10 μM. Binding constants (K_ds) were calculated with a standard dose-response curve using the Hill equation:
Response = Background + Signal - Background
1 + (K_d Hill Slope / DoseHill Slope)
The Hill Slope was set to -1.
Curves were fitted using a non-linear least square fit with the Levenberg-Marquardt algorithm.

Computational modelling

Predicted structure models of the *in cis* and *in trans* complexes were built from the crystal structure of **3**. The BD2 domain was constructed through homology with the second BD1 domain of the crystal structure and the interdomain region was constructed using MOE homology model builder (Chemical Computing Group, Montreal, QC, Canada) with default parameters. The relative positioning of the two pairs of domains for the in trans model was chosen so as to place the relevant termini approximately as far apart as they appear in the *in cis* model.

NMR spectroscopy

All NMR experiments were performed at 30 °C on a Bruker Avance III 800 MHz (18.8 T) spectrometer running TopSpin v3.2 and equipped with a 5mm z-gradient $^{1}H/^{13}C/^{15}N$ TCI probe. The NMR sample used for the titrations contained 0.03 mM of **6** or 0.14 mM of **1** uniformly $^{2}H,^{15}N$-labeled BRD4(44-460) in 20 mM Na_2HPO_4, 2 mM TCEP (tris(2-carboxyethyl)phosphine), and 7%/93% D_2O/H_2O at pH 6.7. Unlabelled compounds **1** and **6** were dissolved in DMSO to give a final concentration of 100 mM and were subsequently titrated into the protein sample to give ligand:protein stoichiometries of 0:1, 1:1 and 2:1. Data sets were processed using the program nmrPipe[52] and plotted using the Python program nmrGlue[53].
The distinction between the two BRDs was accomplished through comparisons with 2D TROSY HSQC spectra of isolated BRD4(1) and BRD4(2). BD1 has three tryptophans in its sequence, whereas BD2 contains one (W374), with indole nitrogen ^{1}H resonances located between 9.6 and 10.5 ppm. Hence, by comparing the spectra of isolated BRD4(2) and BRD4(1,2) (**Supplementary Fig. 7b**), the signal for W374 was directly assigned.

Analytical Ultracentrifugation

Protein samples of BRD4(40-169) and BRD4(1-477) were characterised by sedimentation velocity analytical ultracentrifugation. Samples of protein of ~50 μM concnetration were initially analysed and buffer exchanged on a Superdex200 gel filtration column (GE), coupled to a Wyatt multi-angle light scattering detector (MALLS), a refractive index detector and UV detector, which was equilibrated in 10 mM Tris pH 7.4, 150mM NaCl. This performed buffer exchange and allowed analysis of sample heterogeneity and mass.
All compounds were separately dissolved to a concentration of 1 mM in 100% DMSO. Protein samples were diluted in 10mM HEPES pH 7.4, 150mM NaCl to final concentrations of ~20 μM for BRD4 40-169, and 8 or 11 uM for BRD4(1-477). The final concentration of compounds was adjusted to compound:protein molar ratios of 2:1, 1:1, 0.5:1 and 0:1 by addition to the above protein samples. 400 uL of each of the above samples were loaded into 2-sector epon centrepieces with sapphire glass and were centrifuged at 50,000 rpm in a Beckman XL-I ultracentrifuge at 20 °C collecting scans every 1 minute until sedimentation of the protein was reached. Data was analysed using the sedimentation distribution modelling software Sedfit (REF), and used to calculate the frictional ratio (f/f_0) from the frictional coefficient (f) and that of a sphere (f_0). Analysis of continuous c(s, f/f_0) contour analysis was performed within Sedfit.

Small angle X-ray scattering

The synchrotron radiation X-ray scattering data from solutions of truncated BRD4 construct containing two bromodomains were collected in two experimental sessions at the beamline BM29 at the European Synchrotron Radiation Facility (ESRF, Grenoble)[54]. Using a Pilatus 1M detector at a sample to detector distance of 2.867 m and a wavelength of $\lambda = 0.09919$ nm, the range of momentum transfer $0.05 < s < 5.0$ nm^{-1} was covered ($s = 4\pi \sin\theta / \lambda$, where 2θ is the scattering angle). The apo protein

solutions and those containing test compounds were measured at concentrations 1, 2, 5 and 10 mg/ml using a continuous flow cell capillary. To monitor for the radiation damage, 50 successive 0.2 s exposures of protein solutions were compared and frames with statistically significant changes were discarded. The data were normalized to the intensity of the transmitted beam and radially averaged; the scattering of the buffer was subtracted and the difference curves were scaled for protein concentration. The low angle data measured at lower protein concentrations were extrapolated to infinite dilution and merged with the highest concentration data to yield the final composite scattering curves.
The forward scattering I(0), the radius of gyration R_g along with the distance distribution function of the particle p(r) and the maximum dimension D_{max} were derived using the automated SAXS data analysis pipeline[55]. The p(r) functions were further recomputed manually with the program GNOM[56]. The molecular masses (MM) were evaluated by comparison of the forward scattering with that from a bovine serum albumin (MW = 66 kDa) reference solution.
Ab initio shape models of the BRD4 constructs were generated using the bead modelling program DAMMIN[57]. This program represents the particle shape by an assembly of densely packed beads and employs simulated annealing to construct a compact interconnected model fitting the experimental data. Multiple runs were performed to generate 15-20 models.
Using the Ensemble Optimization Method (EOM)[22], a pool of 10 000 models comprising two rigid bromodomains (residues 42-168, PDB ID: 2oss and 349-458, PDB ID: 2yem) connected by a flexible linker, N-terminal tag and flexible N- and C-termini were generated. The scattering from each model from the pool was calculated with the program CRYSOL[58]. A subset of the pool was selected using a genetic algorithm such that the calculated averaged scattering of the selected models agreed with the experimental data. The R_g distributions of the selected ensembles were obtained by repeating the selection process multiple times. For the 100 models best fitting the experimental scattering from each construct the histograms of the distances between the centres of the two bromodomains were computed. For the top fitting model for each construct best the sedimentation coefficients were computed using WinHydroPro v.1.00[59].
1% DMSO was added to the inhibitor-containing solutions to improve their solubility. To verify that DMSO does not influence the results the apo protein was measured in 0%, 1% and 10% DMSO; after subtraction of the scattering of the appropriate DMSO-containing buffers it was found that DMSO addition does not affect the SAXS profile.
All samples were measured at solute concentrations 1, 2, 5 and 10 mg/ml. A significant concentration dependence was observed for all samples indicating increased protein aggregation or oligomerisation with concentration. The magnitude of the concentration effect was different for the different constructs. For the apo protein data (**Supplementary Fig. 17a**) the effect was moderate indicating some degree of oligomerization (quantitatively, moderate dimerization). A similar albeit somewhat larger effect is observed in the presence of **1**. For **6** (**Supplementary Fig. 17b**), the concentration effect was much more pronounced indicating formation of significant amounts of larger oligomers (tetra- octa- and even largrer). The data from all these concentration series were extrapolated to infinite dilution and the further analysis for all constructs was performed on the extrapolated data, which are expected to correspond to monomeric species (**Supplementary Fig. 18**). The p(r) function of the apo protein has a skewed shape typical for very elongated structures, with the maximum corresponding to the particle cross-section (about 4 nm). From experimental data from the apo protein and from the mixtures with the ligands **1** and **6**, each at three stoichiometries (ligand:protein, 0.5:1, 1:1 and 2:1), extrapolated to infinite dilution, distance distribution functions were calculated using GNOM[56]. The overall structural parameters apparent molecular mass (MM) computed from forward scattering, the radius of gyration (R_g) and the maximum particle dimension (D_{max}) were extracted from the extrapolated curves (**Supplementary Table 8**).
A further and more detailed analysis of the results was performed using BRD4 sequence information. The available crystal structures of the bromodomains (PDB ID: 2oss and 2yem) correspond to residues 42-168 and 349-458 in the full-length construct, which consists of: His-tag (24 aa) + N-terminus (41 aa), BD1 domain (127 aa), a 180 aa long inter-domain linker, domain BD2 (111 aa), C-terminus (18 aa).
According to the NORSnet prediction[60], residues 1-60 and 168-351 are likely to be disordered. Therefore, it appeared likely that BRD4 is flexible in solution and appropriate analysis methods should be used to account for that. We employed the Ensemble Optimization Method (EOM), a

technique where a large pool of randomized models is generated and sub-ensembles are selected in such a way that their mixtures fit the experimental data[22]. 10 000 models were generated keeping the crystal structures of the domains intact and randomizing the linkers. The properties of the system could be inferred from the analysis of the distributions of the overall parameters (e.g. R_g and interdomain distance) in the selected ensembles compared with the random pool.

Bioluminescence Resonance Energy Transfer assay (BRET) NanoBRET assay

Studies were performed using HEK293 or HCT116 cells. HEK293 human embryonic kidney cell line or from the American Type Tissue Culture Collection (ATCC; CCL-247) were cultured in DMEM medium containing 2mM glutamine and 10% foetal calf serum. HCT 116 human colorectal carcinoma cells from the American Type Tissue Culture Collection (ATCC; CCL-1573) were cultured in McCoy's 5A medium containing 2mM glutamine and 10% foetal calf serum. Cells (8 x 10^5) were seeded into wells of a 6-well culture plate (Corning) and allowed to attach for 6 hours. They were then co-transfected with Histone H3.3-Halotag (NM_002107) and either NanoLuc-BRD4 full-length (1-1362) (060885), NanoLuc-BRD4 full-length N433F mutant, or NanoLuc-N-terminal BRD4-BD1 (amino acids 44-168) expression vectors (Promega). For intramolecular biosensor experiments, cells were transfected with a Halotag-BRD4-BD1_BD2-NanoLuc (amino acids 44-460) fusion or a Halotag-BRD4-BD1(N140F)_BD2-NanoLuc mutant fusion expression vectors (Promega). Twenty hours post-transfection, cells were harvested and resupended in OptiMEM (Life Technologies) supplemented with 4% foetal calf serum at a density of 2 x 10^5 cells/ml in the absence (control) or presence (experimental) of 100nM HaloTag NanoBRET 618 fluorescent ligand (Promega). Cells were then seeded into white, flat bottomed tissue culture-treated plates (Greiner), 90 µl cell suspension per well, to which test compounds or vehicle (final DMSO concentration 0.1% (v/v)) were added as 10 fold solutions in complete media at various concentrations. Plates were incubated for 18 hours at 37°C in the presence of 5% CO_2. NanoBRET Nano-Glo Substrate (Promega) was added to both control and experimental samples at a final concentration of 10 µM. Plates were read within 10 minutes using a CLARIOstar plate reader (BMG Labtech) equipped with a 450/80nm bandpass and 610nm longpass filter module. A corrected BRET ratio was calculated, defined as the ratio of the emission at 610nm/450nm for experimental samples (i.e. those treated with HaloTag NanoBRET 618 fluorescent ligand) subtracted by the emission at 610nm/450nm for control samples (i.e.those not treated with HaloTag NanoBRET 618 fluorescent ligand). BRET ratios were expressed as milliBRET units (mBU), where 1 mBU corresponds to the corrected BRET ratio multiplied by 1000.

Cell Transfection, Treatments, and Quantitative NanoBRET Target Engagement Measurements Under Equilibrium Conditions

Target engagement at NanoLuc-BRD4 was performed as described previously[26]. For determining unlabeled compound isotherms, the iBET-NCT tracer was added to the cells at a fixed concentration of 0.2 µM prior to test compound addition. Serially-diluted test compounds were then added to the cells and allowed to equilibrate for 3 hr prior to BRET measurements. To measure BRET, NanoBRET NanoGlo Substrate-(Promega) was added, and filtered luminescence was measure on a Promega Glomax Discover luminometer equipped with 450 nm BP filter (donor) and 610 nm LP filter

(acceptor), using 0.5 s integration time. Competitive displacement data were then graphed with GraphPad Prism software using a 3-parameter curve fit with the following equation;
Y=Bottom + (Top-Bottom)/(1+10^((X-LogIC$_{50}$)))
Normalized data were generated by assigning 100% to the maximum of the 3-parameter curve fit and 0% for the theoretical minimum value of the 3-parameter curve fit.

$$K_i = \frac{IC_{50}}{1 + \frac{[L]}{K_D}}$$

Kinetic Analysis of Intracellular Residence Time at BRD4 via NanoBRET

For direct analysis of relative compound dissociation rates via BRET, 2 x 10^6 cells transfected with NLuc-BRD4 constructs were processed as described previously[26]. Briefly, transfected cells were first pre-equilibrated with test compound for 3 hr at 37°C/5% CO_2. Cells treated with compound were pelleted, washed once with PBS, and resuspended in 10 mL of Opti-MEM in the presence of NanoBRET NanoGlo Substrate and 1 µM iBET-NCT tracer immediately prior to BRET measurements. BRET data were normalized to 100% signal from the positive control (defined as the maximum BRET value observed from cells treated with 1uM iBET-NCT in the absence of unlabeled competing compound) and 0% signal (defined as the BRET value observed from cells treated with 1 uM iBET-NCT + 10 µM unmodified **1**).

Cell lines

All cell lines were originally purchased from ATCC or DSMZ, cultured following vendors' instruction and authenticated using DNA fingerprinting short-tandem repeat (STR) assay and tested to be free of mycoplasma contamination. All revived cells were used within 15 passages and less than 6 months.

Immuno-fluorescent, foci assays for BRD4, MED1, and H3K27Ac

U2OS cells were plated in 96-well plates at 16,000 cells/well. Cells were incubated at 37°C in 5% CO_2 overnight and then dosed with compounds at indicated concentrations for 4hr. DMSO was used as a max control. Cells were fixed by 4% formaldehyde at room temperature (RT) for 10 minutes and followed by 0.1% saponin permeabilization for another 10 minutes. Cells were co-stained by anti-BRD4 antibody (1:25, Sigma Aldrich HPA015055-100UL) with either anti-MED1 antibody (1:50, Bethyl Laboratories A303-876A) or anti-H3K27Ac antibody (1:250, Diagenode C15200184) for 2 h at 37°C, washed with PBS for four times, and labelled by Alexa Fluor 488 anti-rabbit with either Alexa Fluor 594 anti-goat antibody or Alexa Fluor 594 anti-mouse antibody at 1:200 dilution (life Technology) for 1 h at RT. After washed with PBS twice, cells were stained with Hoeschst at 1:4000 (life Technology, H21492) for 10 minute, washed twice with PBS and then subjected to image acquisition by ImageXpress MicroXL High Content Screening System (Molecular Devices). The data was analyzed by MetaXpress (Molecular Devices). IC_{50} was calculated using GraphPad Prism.

c-Myc flow assay

MM.1S cells were plated in 96-well plates at 200k cells/well and treated with serial concentrations of compound 1 h after plating and grown for 16 h at 37°C. Cells were transferred into a 96-well V-bottom plate and fixed sequentially with 2% paraformaldehyde for 10 min at 37°C followed with 90% cold methanol for 10min on ice. Cells were washed and blocked in incubation buffer (PBS+0.5%BSA) for 10 min and incubated with anti-c-Myc primary antibody (1:200, Cell Signalling Technology #5605) at RT for 1 h. Cells were washed twice and then stained with Alexa 488 conjugated anti-rabbit IgG (1:1000, Cell Signalling technology #4412) for 30 min at RT and washed again. The pellet was resuspended in incubation buffer and analyzed by flow cytometer (BD FACSCalibur) using the FL-1 detector. Data was analyzed using FlowJo software V7. Live cell

population was selected by gating on FCS/SSC and Geo Mean fluorescence of FL-1 signal was used to calculate IC_{50}s.

Western blot experiments

4 x 10^6 MM.1S cells were seeded in each well of the 6-well plates and treated with compounds at various concentrations for 4h. Crude lysate was prepared with 1xSDS lysis buffer (0.06 M Tris-HCl pH6.8, 1% SDS, and 10% glycerol). Samples with 20 µg of total protein were loaded and Western blots were run following typical procedures. Primary c-Myc antibody (CST #5605) was used at 1:1000 dilution, GAPDH antibody (CST #5174) at 1:10,000 dilution, and secondary anti–rabbit HPR-conjugated antibody (CST) at 1:10000 dilution. Protein level was visualized using the ImageQuant LAS4000.

Cell growth inhibition and viability assays

Optimal 384w seeding densities were pre-measured for linear growth over 72hr. 30ul cells/well were seeded in black, flat bottom 384w plates and treated with compounds for 72hr. The viable cells were measured using Alamar Blue reagents following manufacture's protocol (Invitrogen) and the % viable cells were calculated by comparing to no-drug controls. The percent net growth is calculated by normalising against the no-drug controls, and the GI_{50} value, the concentration that causes 50% net growth inhibition, was calculated using GraphPad Prism 6.

Viability assay was performed following the same protocol as the growth inhibition assay but differed in data treatment. Absolute number of remaining viable cells, instead of percent net growth, was determined after 72 hours of compound treatment. Dose-response curves were plotted in GraphPad Prism and fitted using sigmoidal nonlinear regression to determine IC_{50} values.

Gene expression analysis by RNA-seq

To compare the genome-wide transcriptional consequences induced by the different BET inhibitors, we performed RNA-sequencing on hematologic cancer cell lines (K-562, MM.1S, MV-4-11, obtained from the American Type Culture Collection) after treatment with **1** (2 uM), **6** (0.05 uM) or DMSO control for 24 hours. Correlation analysis of the gene expression changes after inhibitor treatment revealed that the gene abundance differential strongly correlates between all compounds indicating that the transcription profile of each inhibitor is similar.

After BET inhibitor (6 - 0.05 uM, 1 – 2 uM,) or DMSO vehicle treatment of cell lines (MV-4-11, MM.1S, K-562) for 24 hours, RNA isolation, cDNA library generation, and sequencing to 12M reads on the Illumina HighSeq was carried out at Q2 Solutions (http://www.q2labsolutions.com/). Bcbio-nextgen (https://github.com/chapmanb/bcbio-nextgen) was used to process FastQ files, perform quality control, alignment to genome build hg38 using HISAT2[61], and quantify transcription

expression based on Ensembl annotation. DESeq2[62] version 1.12.1 was used to identify differentially expressed genes and calculate $\log_{10}$FoldChange values (**Supplementary Fig. 19**).

Methods-only references

42. Buttar, D. *et al*. *Bioorg. Med. Chem.* **8**, 7486-7496 (2010)
43. Camenisch, G. *et al. Eur. J. Pharm. Sci*. **6**, 313-319 (1998)
44. Kabsch, W. *Acta Cryst*. **D66**, 125-132 (2010)
45. McCoy, A.J. *et al. J. Appl. Cryst*. **40**, 658-674 (2007)
46. Emsley, P. *et al*. *Acta Cryst*. **D66**, 486-501 (2010)
47. Bricogne, G. *et al.* Buster version 2.11.6. Cambridge, United Kingdom: Global Phasing Ltd. (2011)
48. Smart, O.S. *et al.* Grade version 1.2.9. Cambridge, United Kingdom: Global Phasing Ltd. (2011)
49. Callis, R. *et al. J. Biomol. Screen*. **20**, 748-759 (2015)
50. Zhang *et al*. *J. Biomol. Screen*. **4**, 67-73 (1999)
51. Zava *et al*. *Endocrinology*, **104**, 1007-1012 (1979)
52. Delaglio, F. et al. *J. Biomol. NMR*. **6**, 277-293, (1995)
53. Helmus, J.J. & Jaroniec, C.P. *J. Biomol. NMR*. **55**, 355-367 (2013)
54. Pernot, P. *et al*. *J. Synchrotron Radiat*. **20**, 660–664 (2013)
55. Franke, D., Kikhney, A.G. & Svergun, D.I.. *Nuc. Inst. Meth. A*. **689**, 52-59 (2012)
56. Svergun, D.I. *J. Appl. Cryst*. **25**, 495-503(1992)
57. Svergun, D.I., *Biophys. J*. **76**, 2879-2886 (1999)
58. Svergun, D.I., Barberato, C. & Koch, M.H.J. *J. Appl. Cryst*. **28**, 768-773 (1995)
59. Ortega, A., Amorós, D. & García de la Torre, J. *Biophys J*. **101**, 892-898 (2011)
60. Schlessinger, A., Liu, J. & Rost, B. *PLoS Comput Biol.* **3**, e140 (2007)
61. Kim, D., Langmead, B., Salzberg, S.L. *Nat. Methods.* **12**, 357-360 (2015)
62. Love, M.I., Huber, W., Anders, S. *Genome Biol*. **15**, 550 (2014)

Competing financial interests

The work described here was initiated as a project within AstraZeneca. MJW, AAR, GW, RHB, DO and JP are former employees of AstraZeneca and may hold stock in the company. HC, RB, SB, RC, EC, ID, AD, LF, GH, MMcA, PP, GRR, SS, NS, WW, DW, DMW and YY are employees of AstraZeneca and may hold stock in the company. Promega Corp. carried out the nanoBRET experiments as part of a collaboration with AstraZeneca. DLD, JM and MBR and employees of Promega Corp. and may hold stock in the company. The University of Manchester carried out the AUC studies at the request of AstraZeneca. TAJ is an employee of the University of Manchester. The European Molecular Biology Laboratory carries out the SAXS studies at the request of AstraZeneca. AK and DIS are employees of the European Molecular Biology Laboratory.

a)

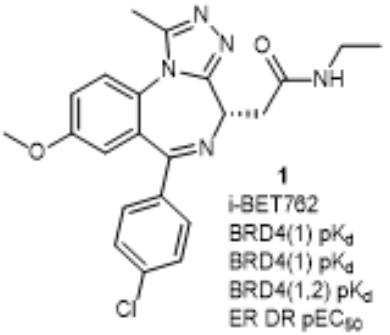

1
i-BET762

BRD4(1) pK_d	7.5
BRD4(1) pK_d	7.8
BRD4(1,2) pK_d	7.8
ER DR pEC_{50}	6.3
cMyc DR pEC_{50}	6.6

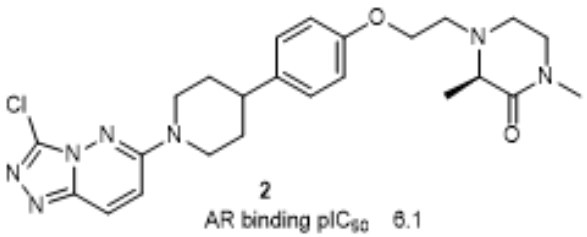

2

AR binding pIC_{50}	6.1
AR DR pEC_{50}	7.6
ER binding pIC_{50}	<4.0
ER DR pEC_{50}	7.4
BRD4(1) pK_d	7.2
BRD4(2) pK_d	6.1
BRD_4(1,2) pK_d	6.4
cMyc DR pEC_{50}	7.1

b)

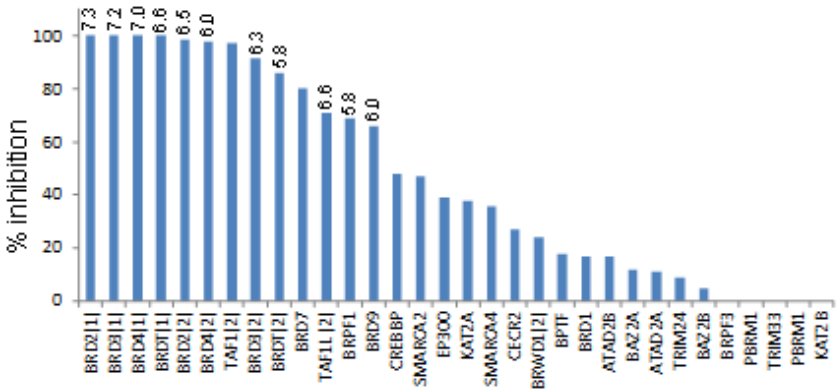

c)

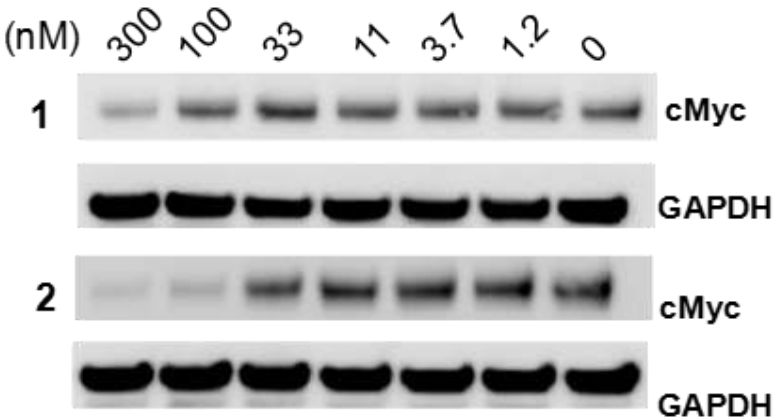

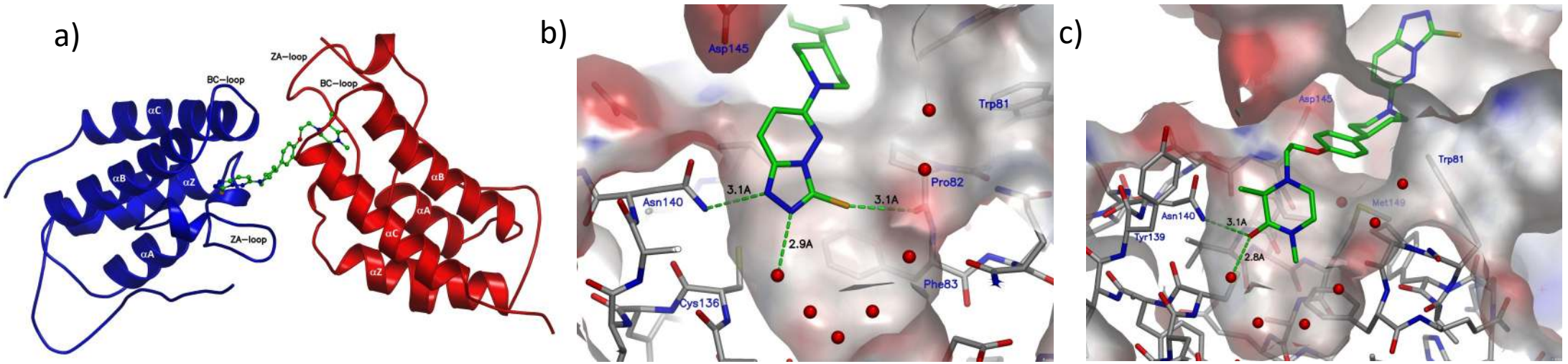
a)
ZA–loop
BC–loop
BC–loop
αC
αB
αZ
αA
ZA–loop
αB
αA
αC
αZ
b)
Asp145
Trp81
Pro82
3.1A
3.1A
Asn140
2.9A
Phe83
Cys136
c)
Asp145
Trp81
Met149
Asn140
3.1A
Tyr139
2.8A

a)

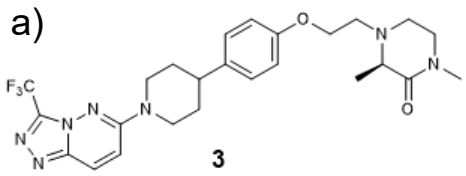

3

BRD4(1) pK_d	6.7
BRD4(2) pK_d	5.7
ER DR pEC_{50}	7.7
cMyc DR pEC_{50}	7.1

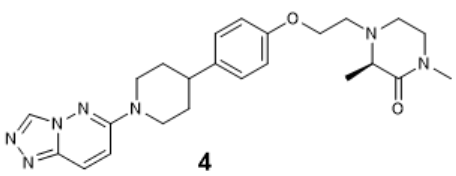

4

BRD4(1) pK_d	5.3
BRD4(2) pK_d	5.1
ER DR pEC_{50}	<5.5
cMyc DR pEC_{50}	5.9

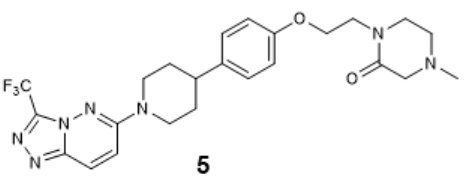

5

BRD4(1) pK_d	6.7
BRD4(2) pK_d	5.4
ER DR pEC_{50}	<5.5
cMyc DR pEC_{50}	ND

b)

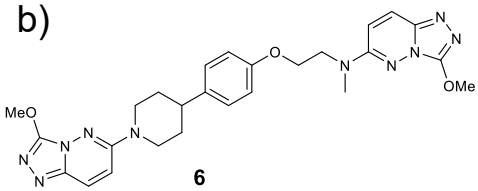

6

BRD4(1) pK_d	8.1
BRD4(2) pK_d	7.3
BRD4(1,2) pK_d	11
ER DR pEC_{50}	9.2
cMyc DR pEC_{50}	9.2

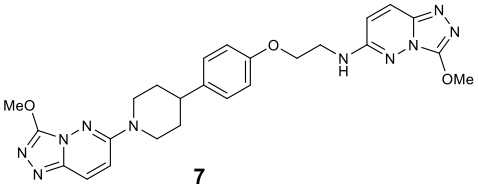

7

BRD4(1) pK_d	8.9
BRD4(2) pK_d	8.1
BRD4(1,2) pK_d	11
ER DR pEC_{50}	9.7
cMyc DR pEC_{50}	>9.3

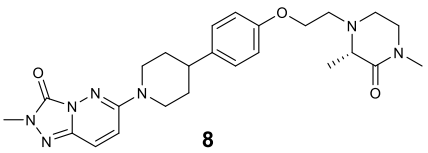

8

BRD4(1)	inactive at 10 μM
BRD4(2)	inactive at 10 μM
ER DR	inactive at 30 μM

c)

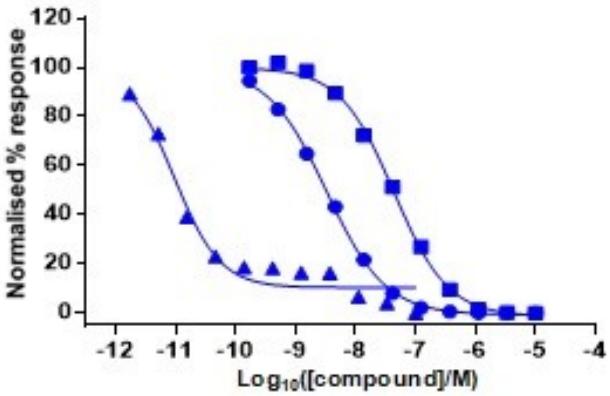

d)

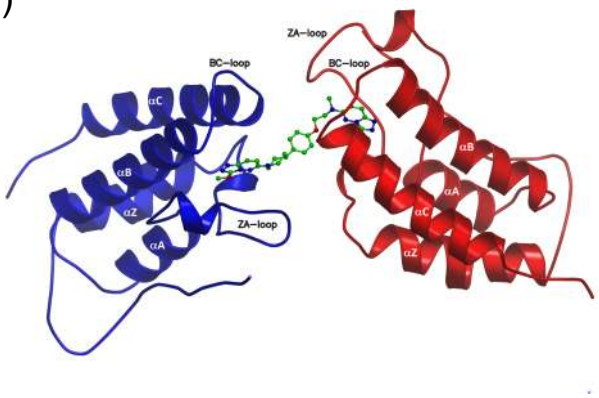

a)

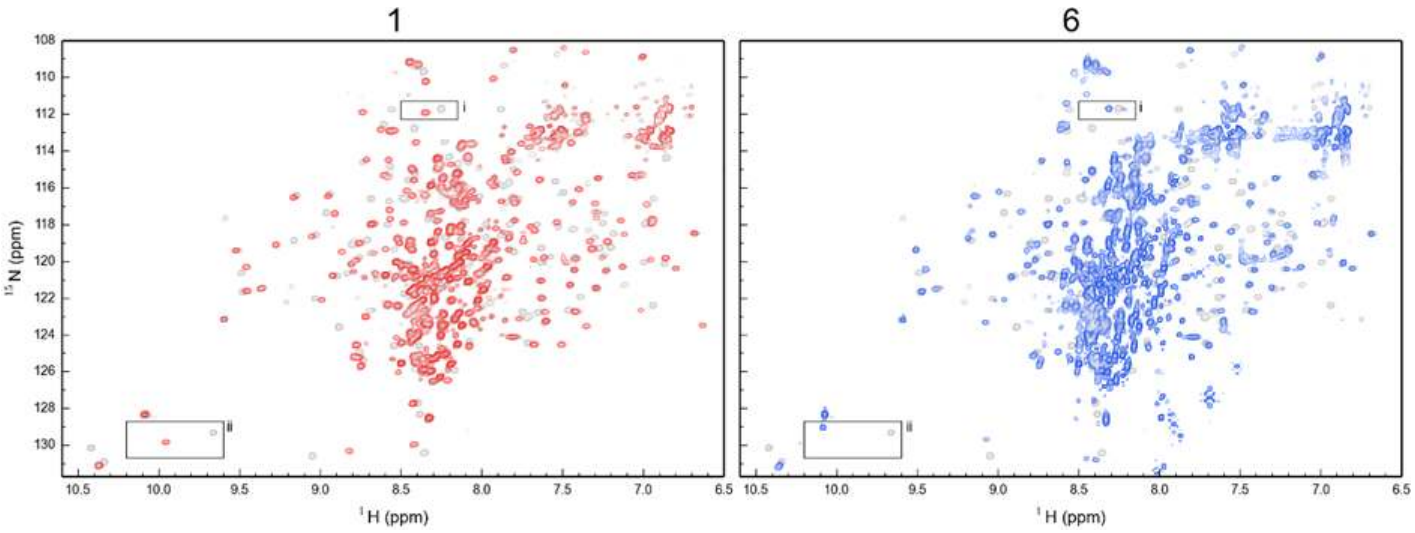

b)

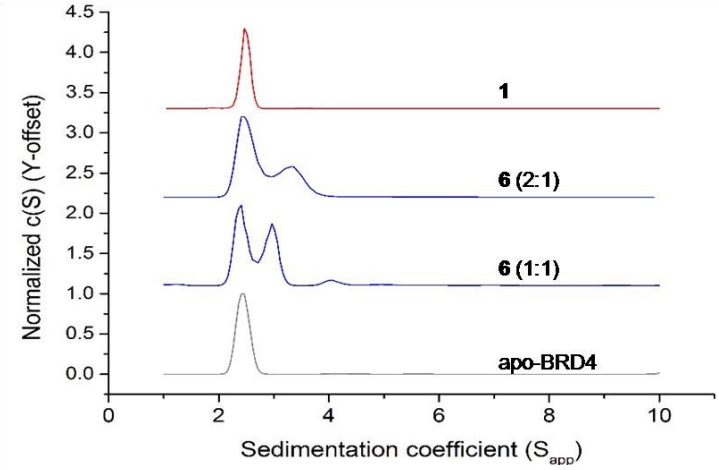

c)

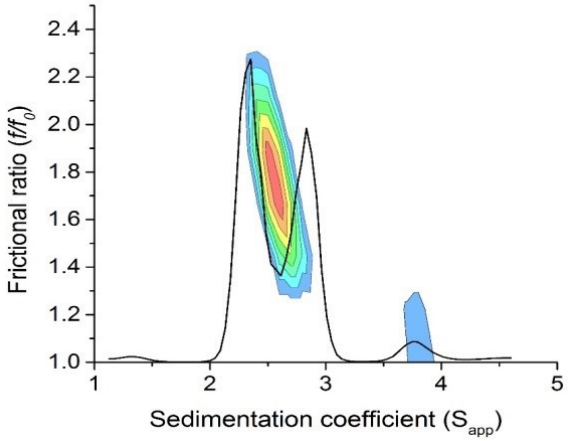

d)

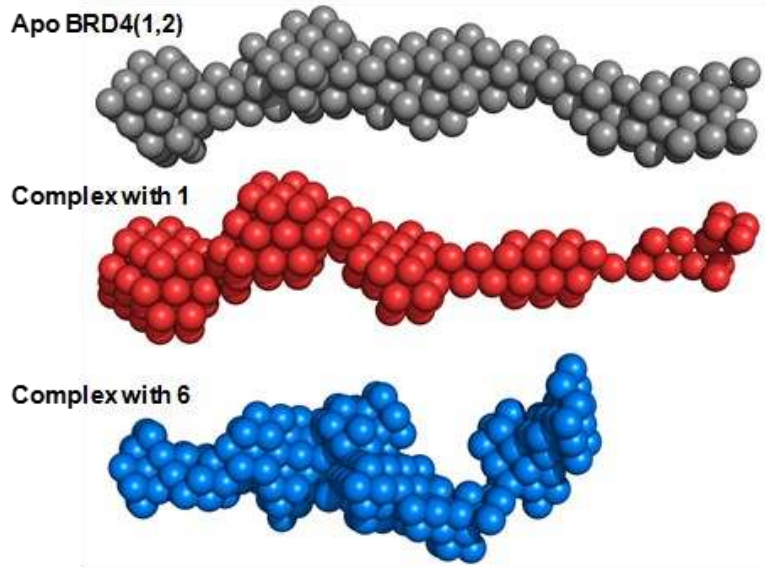

	Interdomain distance / Å
Apo BRD4(1,2)	140 ± 12
Complex with 1	150 ± 12
Complex with 6	63 ± 18

a)

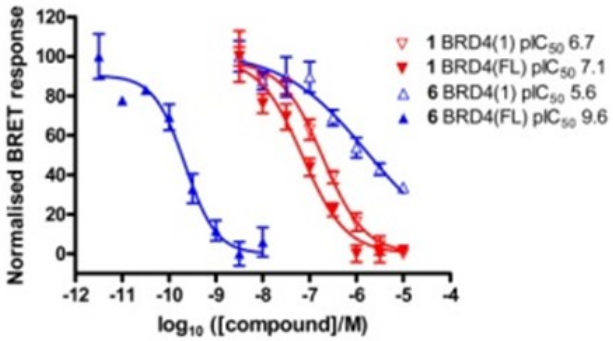
Normalised BRET response
log10 ([compound]/M)
1 BRD4(1) pIC50 6.7
1 BRD4(FL) pIC50 7.1
6 BRD4(1) pIC50 5.6
6 BRD4(FL) pIC50 9.6

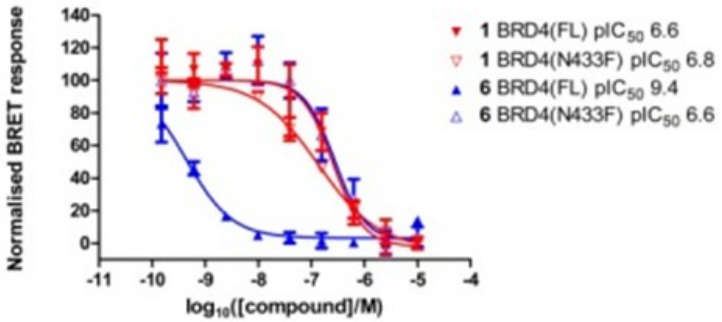
Normalised BRET response
log10([compound]/M)
1 BRD4(FL) pIC50 6.6
1 BRD4(N433F) pIC50 6.8
6 BRD4(FL) pIC50 9.4
6 BRD4(N433F) pIC50 6.6

b)

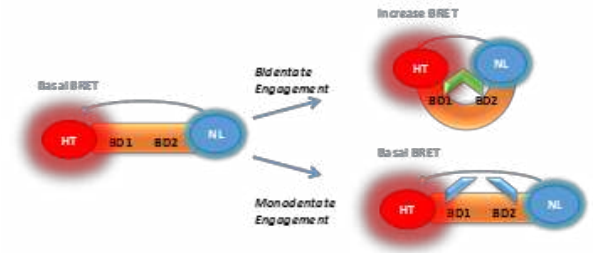
Basal BRET
Bidentate Engagement
Increase BRET
Monodentate Engagement
Basal BRET
HT
BD1
BD2
NL

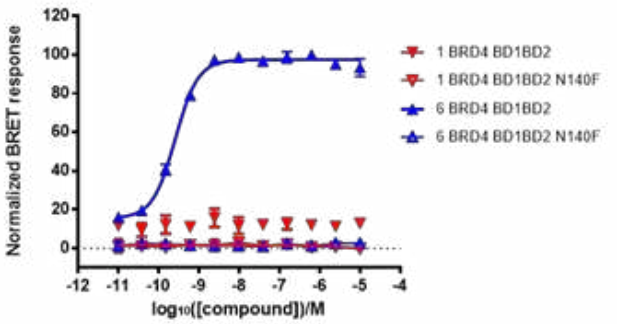
Normalized BRET response
log10([compound])/M
1 BRD4 BD1BD2
1 BRD4 BD1BD2 N140F
6 BRD4 BD1BD2
6 BRD4 BD1BD2 N140F

c)

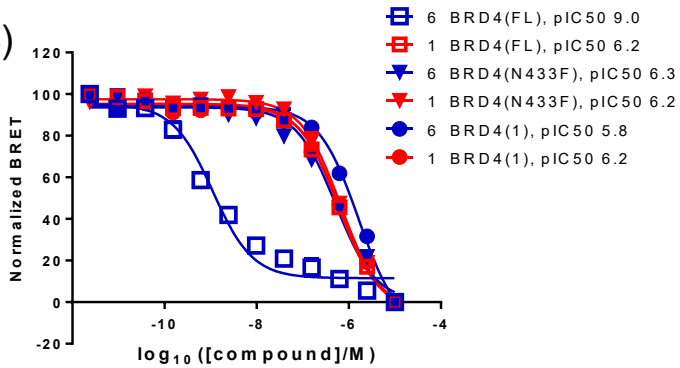
Normalized BRET
log10 ([compound]/M)
6 BRD4(FL), pIC50 9.0
1 BRD4(FL), pIC50 6.2
6 BRD4(N433F), pIC50 6.3
1 BRD4(N433F), pIC50 6.2
6 BRD4(1), pIC50 5.8
1 BRD4(1), pIC50 6.2

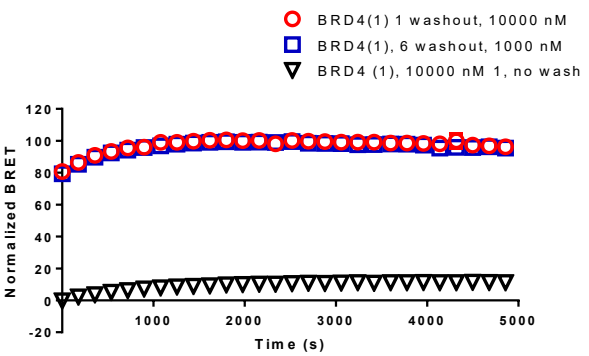
Normalized BRET
Time (s)
BRD4(1) 1 washout, 10000 nM
BRD4(1), 6 washout, 1000 nM
BRD4 (1), 10000 nM 1, no wash

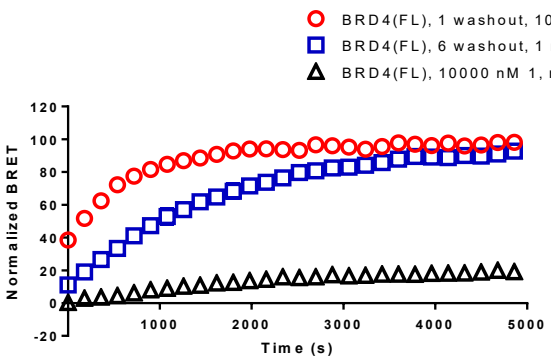
Normalized BRET
Time (s)
BRD4(FL), 1 washout, 10000 nM
BRD4(FL), 6 washout, 1 nM
BRD4(FL), 10000 nM 1, no wash

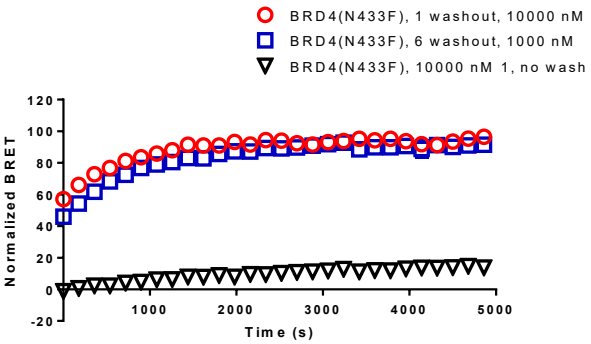
Normalized BRET
Time (s)
BRD4(N433F), 1 washout, 10000 nM
BRD4(N433F), 6 washout, 1000 nM
BRD4(N433F), 10000 nM 1, no wash

a)

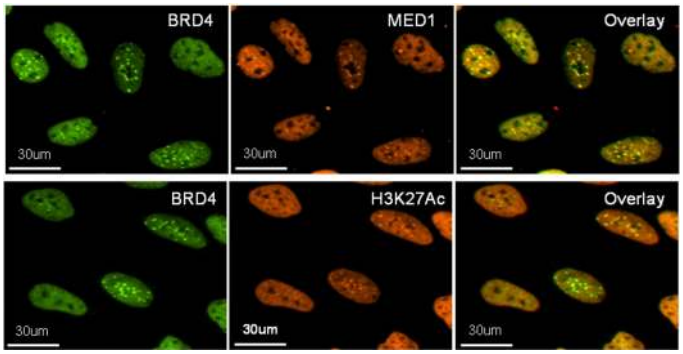
BRD4
MED1
Overlay
BRD4
H3K27Ac
Overlay
30um

b)

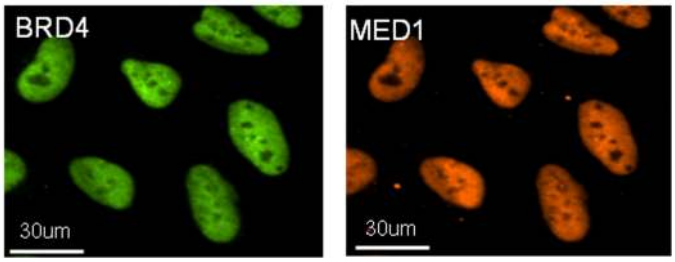
BRD4
MED1
30um
30um

c)

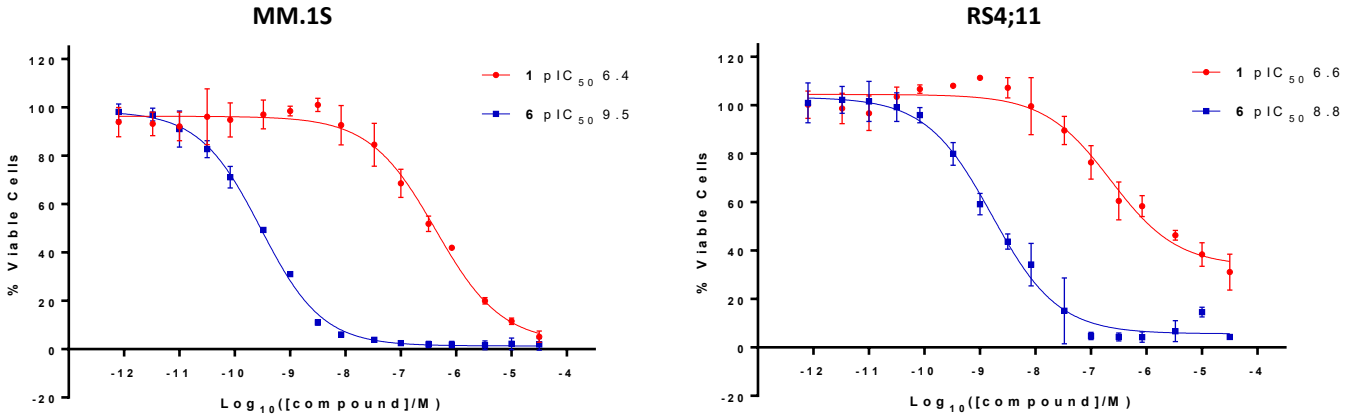
MM.1S
RS4;11
% Viable Cells
Log10([compound]/M)
1 pIC50 6.4
6 pIC50 9.5
1 pIC50 6.6
6 pIC50 8.8

d)

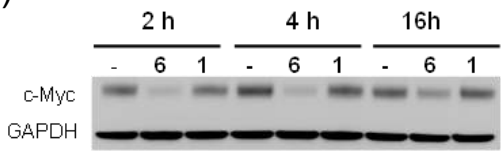
2 h
4 h
16h
- 6 1 - 6 1 - 6 1
c-Myc
GAPDH